International Journal of Fracture **130:** 517–555, 2004.

Effects of atoms on brittle fracture

M. MARDER
Center for Nonlinear Dynamics and Department of Physics
The University of Texas at Austin

Received 21 April 2004; accepted in revised form 20 July 2004

Abstract. This article aims to answer two related sets of questions. First: *in principle, how large an effect can structure at the atomic scale have upon the fracture of two macroscopically identical samples?* The answer to this question is that the effects can be very large. Perfectly sharp cracks can be pinned and stationary under loading conditions that put them far beyond the Griffith point. Crack paths need not obey the rule $K_{II} = 0$. Crack speeds can vary from zero to the Rayleigh wave speed under identical loading conditions but depending upon microscopic rules. These conclusions are obtained from simple solvable models, and from techniques that make it possible to extrapolate reliably from small numerical calculations to the macroscopic limit. These techniques are described in some detail. Second: *in practice, should any of these effects be visible in real laboratory samples?* The answer to this second question is less clear. The qualitative phenomena exhibited by simple models are observed routinely in the fracture of brittle crystals. However, the correspondence between computations in perfect two-dimensional numerical samples at zero temperature and imperfect three-dimensional laboratory specimens at nonzero temperature is not simple. This paper reports on computations involving nonzero temperature, and irregular crack motion that indicate both strengths and weaknesses of two-dimensional microscopic modeling.

Key words: Fracture, atomic models

1. Introduction

Fracture mechanics provides a brilliant framework within which to describe fracture, but there are some questions that it does not have to answer. Fracture mechanics calculations direct one to isolate a process zone surrounding the crack tip. Outside of this zone, a material obeys equations of linear elasticity, and the stress singularities near the crack tip adopt a universal form. Somewhere within it, atomic bonds rip apart, and cracks move ahead straight,or turn, or branch.

The mathematics of fracture mechanics is often thought to ensure that for sufficiently large macroscopically isotropic samples, the environment of a crack tip can be described completely by four real numbers: three stress intensity factors, and the instantaneous crack velocity v.

In addition, one needs information that is particular to the material at hand. At the very least one needs to know the critical energy flux G_c for which the crack tip first begins to move, and elastic constants such as Young's modulus and Y and Poisson's ratio ν.

Given these quantities, here are some predictions one would like to make:

1. Criterion for onset of crack motion.
2. Crack speed along a straight path.
3. Condition for crack to turn away from straight path.
4. Equation of motion for single crack moving along arbitrary path.
5. Criterion for crack branching.
6. Equation of motion for branching cracks, including branching angle.

Here are some possible scenarios describing what might be needed to obtain such predictions:

1. Given the constants G_c, Y, ν, all properties of crack motion are precisely determined for all materials, as a function of G_c, Y, ν, K_I, K_{II}, K_{III}, and v.
2. Given G_c, Y, ν, all properties of crack motion are approximately determined, with small material-dependent corrections.
3. In addition to G_c, Y, and ν a finite number of additional materials constants is needed, after which all crack properties are precisely determined.
4. In addition to G_c, Y, and ν, an additional function describing a cohesive zone is sufficient to predict crack properties.
5. Materials fall into a small number of universality classes. Within each class specifying G_c, Y, ν and a small number of additional constants is enough to determine all properties of crack motion, either exactly or to excellent approximation.
6. Crack motion depends in great detail upon properties of the process zone,and there is no limit to how different two macroscopically identical materials can be.

A first conclusion of this article is that *in principle* case 6 applies. I will provide specific examples of macroscopically identical isotropic elastic samples whose fracture properties are highly variable, with crack speeds and directions depending sensitively upon details at the atomic scale.

The primary tool I will employ to arrive at these conclusion is analytical and numerical solution of atomic models of fracture. Using analytical and numerical results requires that one be able to make a connection with the macroscopic limit of fracture mechanics. The analytical theory is crucial in this respect: it permits exact solution of certain atomic models, but more even more importantly it shows how to assemble data from numerical calculations on small finite systems so as to make macroscopic predictions.

Some additional points on the philosophy of the computations in this paper. The field of fracture has been the setting for remarkable advances in large-scale computation applied to materials science. Abraham (1994) first demonstrated the possibility of performing computations with millions of atoms. Forefront computations now involve billions of atoms. Simultaneously, there has been a substantial effort directed toward finding physically realistic laws for interatomic interactions in particular systems (Holland and Marder 1998a, 1998b, 1999), including fracture simulations that even involve quantum-mechanical computations near the tip (Abraham et al., 2000).

Yet even a billion atoms is a very small number. Either one understands how small-scale computations relate to the macroscopic limit or one does not. If one does, the computation should be carried out in the smallest system making the comparison possible rather than the largest made available by current technology. In addition, realistic potentials are computationally costly, and make it difficult to explore how changing features of the potential affect the phenomenon of fracture. For these reasons, this article will focus exclusively upon simple model potentials. If cracks between atoms obeying these simple potentials disobey fracture mechanics lore, then the lore cannot be fully correct. However, I will try not to shy away from asking, if one could actually build a laboratory sample from atoms obeying these very simple force laws and put it in a tensile-testing machine, what would one see?

2. Energetic considerations

2.1. The Griffith criterion

The idea of energy balance was introduced into the study of fracture by Griffith (1920), and it remains the single most important concept when asking whether when either an experimental or numerical sample can break. Consider an isolated system containing a crack of length l. Compute the potential energy of the system and call the result $U_{\text{tot}}(l)$. Imagine that the crack moves ahead by some small distance dl, and once again compute the potential energy of the sample, $U_{\text{tot}}(l + dl)$. Then fracture is possible if

$$U_{\text{tot}}(l + dl) < U_{\text{tot}}(l) \tag{1}$$

and impossible otherwise. For systems that are are not isolated, for example those in thermal or mechanical contact with external entities, the energy U must be replaced by other potentials.

The form of the energy balance relation (1) is very simple, but it constitutes the fundamental relation from an atomic point of view. In atomic calculations, everything is included when one calculates the energy, including the energies of all the bond-breaking events that let the crack move forward.

The relation may seem more familiar if it is divided into a number of different parts, and one makes a number of assumptions. Draw a loop around the crack tip large enough so that the region outside the loop is completely described by linear elasticity, but small enough that the region inside it is dominated by physics near the crack tip. When the crack tip moves, let this loop move with it, and assume that the energy contained within this loop is independent of the crack tip location. Assume that the energy needed to move the crack tip and the region within the loop around it is proportional to the new surface area opened up by crack motion; define Γ to be the energy per area that provides a coefficient of proportionality. Finally, let $U_{\text{out}}(l)$ be the energy outside of the loop as a function of crack length. Then in a plate of width w (Figure 1), the condition for crack motion becomes

$$U_{\text{out}}(l) + l\Gamma w > U_{\text{out}}(l + dl) + (l + dl)\Gamma w \tag{2}$$

$$\Rightarrow \frac{dU_{\text{out}}}{dl} + \Gamma w < 0 \tag{3}$$

2.2. Energy criteria in a strip

All the studies in this article will be carried out in *thin strip loading*. In this loading configuration, shown in Figure 1, a strip of material is prepared much longer than it is wide. A seed crack is introduced through the center of the strip, and the upper and lower boundaries of the sample are rigidly displaced. Since the boundaries are held fixed during crack motion, the sample is mechanically isolated from the outside world, as assumed in writing down Equation (1).

This loading configuration greatly simplifies the analysis of energy flow because of translational symmetry along the direction of crack motion. The basic symmetry argument that makes this geometry so special is the following: Far ahead of the crack, on the right, the material is uniformly strained. To be definite, consider a slab of length dl, width w, and height h taken from the strip. Suppose that the top of this slab is moved to height δ_y over its equilibrium location, producing a uniform strain in the vertical direction $e_{yy} = \delta_y / h$. Denote the energy needed to produce this strain by

$$U(\delta_y) = h\, dl\, w\, u(e_{yy}). \tag{4}$$

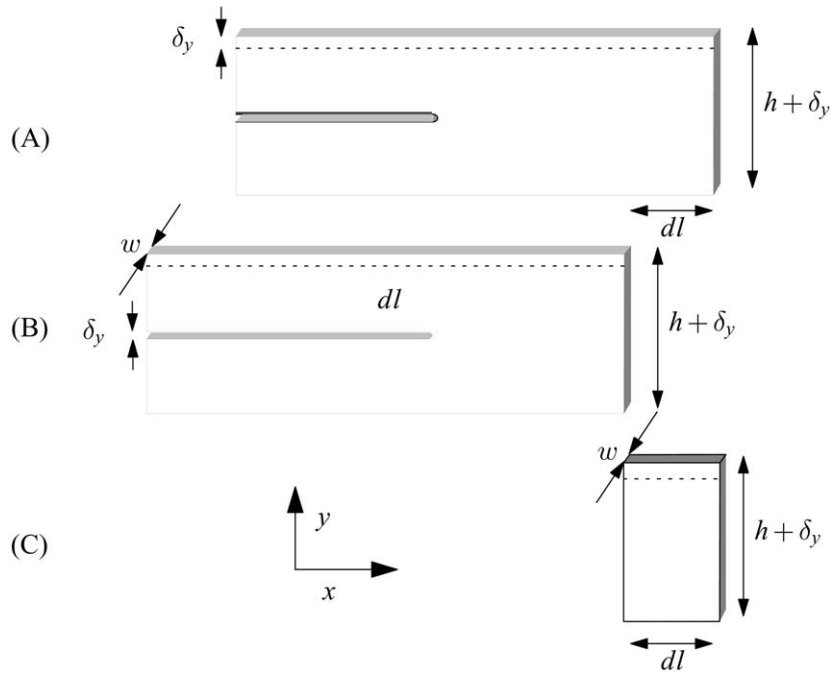

Figure 1. (A) Strip of height h and width w, with top edge rigidly displaced by δy. (B) Crack has moved forward by distance dl. (C) The potential energies of the strips in (A) and (B) differ by the energy stored in the slab depicted here, and by the energy needed to extend the crack through distance dl.

Here $u(e_{yy})$ is the energy per volume resulting from the uniform strain. This scaling form for the energy of a solid remains valid down to atomically small system sizes, so long as as changes at the surface such as surface reconstruction are negligible.

Translational symmetry allows one to determine the minimum value of $u(e_{yy})$ for which fracture becomes energetically possible, employing Equation (1). Consider the relation between panels (A) and (B) in Figure 1. The problems are identical, except that the crack has moved by distance dl, costing energy $\Gamma\, w\, dl$. All the fields around the tip are unchanged in a reference frame that moves with the tip. However, the amount of strained material has been reduced by an amount contained in the slab of length dl. According to the general criterion in Equation (1), fracture is energetically possible when

$$\Gamma\, w\, dl \geq= h\, dl\, w\, u(e_{yy}) \Rightarrow hu(e_{yy}) \geq \Gamma. \tag{5}$$

This criterion is illustrated in Figure 2. The computations are performed for a reasonably realistic silicon potential on a sample just 8 unit cells or 50 Å high. The geometrical construction indicated by Equation (5) is to draw the curve $u(e_{yy})$ and then scale it by h. At the point where the curve hu intersects the horizontal line at Γ, the solid can lower its energy by dividing into two pieces rather than allowing itself to strain further. To the left of this intersection point the strained solid is stable, while to the right of it the cut solid is stable, as indicated in the figure.

All realistic energy functions $u(e_{yy})$ are parabolic for sufficiently small strains e_{yy}. In this limit, one can write

$$u(e_{yy}) = \frac{1}{2} C e_{yy}^2 \tag{6}$$

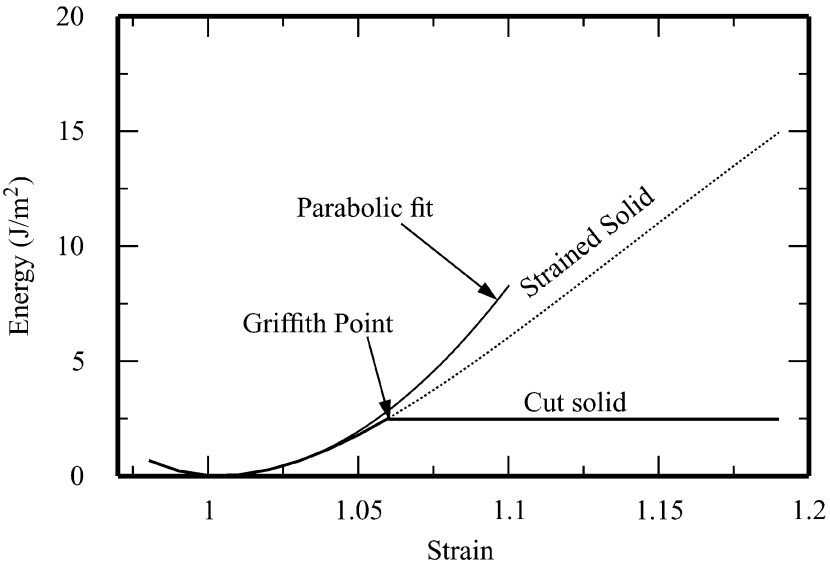

Figure 2. Energy per area hu of a slab of silicon with (111) plane normal to the vertical direction, strained uniformly in vertical direction, compared with energy per area Γ required to cut same slab in half. The slab of silicon is 50.4 Å, or 8 unit cells high. The computations are performed using the Modified Embedded Atom Method potential (Baskes, 1992, Baskes et al., 1994). The solid lines indicate the path of thermodynamic equilibrium as the solid is strained, while the dashed lines indicate when the strained solid, or the solid cut in half, are not thermodynamically favored. A solid whose energy versus extension curve has this form in the macroscopic limit is defined to be brittle.

where C is an elastic constant

Figure 2 illustrates something that is difficult to see outside of numerical work – a system so small that a parabolic fit is not adequately accurate to capture the potential energy curve. At the Griffith point, the parabola exceeds the true energy curve by around 16%. However, for a system twice as high (100 Å) the only change is that the energy curve u must be multiplied by an additional factor of two. The error involved in employing a parabola up to the Griffith point then drops down to 5%. The essential point is that in the macroscopic limit where h becomes large, a generic potential energy u can always be approximated to great accuracy by a parabola over the whole range of strains relevant to fracture.

If the parabolic approximate (6) holds, it is easy to calculate the location of the Griffith point, where cutting the slab in half and straining it have the same energy. This occurs when

$$\Gamma = \frac{1}{2} h C e_{yy}^2 \tag{7}$$

$$\Rightarrow h = \frac{2\Gamma}{C e_{yy}^2} \tag{8}$$

$$\Rightarrow e_{yy} = \sqrt{\frac{2\Gamma}{hC}}. \tag{9}$$

$$\Rightarrow \delta_{yc} = \sqrt{\frac{2\Gamma h}{C}}. \tag{10}$$

In Equation (10), δ_{yc} gives the vertical displacement of the system boundaries needed to stretch it to the Griffith point. The combination Γ/C has dimensions of length. For a brittle material

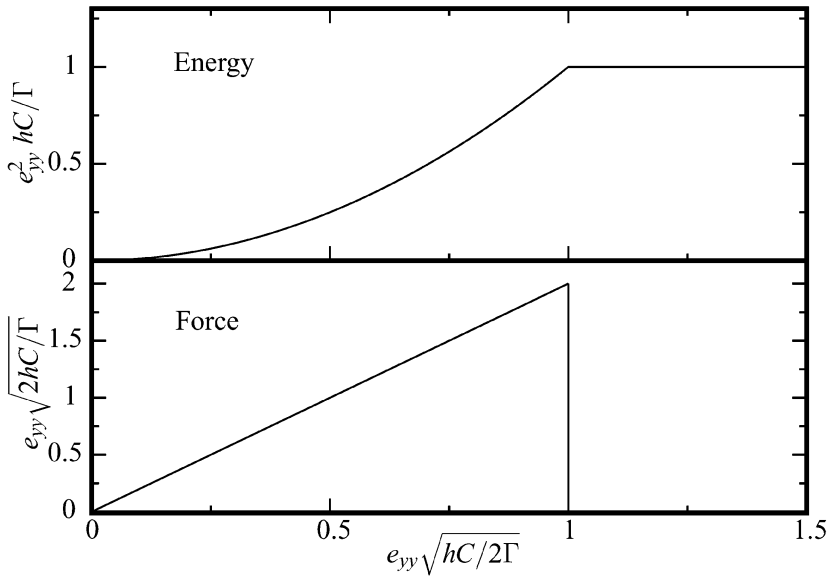

Figure 3. Energy and force required to strain solid vertically, according to Equation (7). These forms describe exactly the thermodynamic equilibrium of all macroscopic solids under strain. Brittle solids are defined to be those for which energy or force measured in the laboratory actually resemble these curves.

such as silicon, it is of order 10^{-11} m, since C is of order 100 GPa, while Γ is of order 1 J/m^2. Linear elasticity typically applies below strains of around 1%. Based upon these estimates, one finds from Equation (8) that linear elasticity should generally become valid far to the right of a crack tip when h is on the order of 100 Å or above. Also note that for h on the order of 10 cm, the displacement δ_{yc} is around 1 μm and strains are on the order of 10^{-6}. This simple calculation provides a first indication that studies of fracture in systems on the order of 100 atoms high are capable of making predictions about fracture in macroscopic samples. The calculations that follow will provide much more detailed evidence for this claim.

2.3. Definition of brittleness

In the thermodynamic limit, a plot of energy per area versus strain for *any solid* is given by Figure 3.The orders of magnitude in the previous section apply to most solids, such as glass or steel. From a purely thermodynamic point of view, 10-cm high samples of either of these solids should split in half when subject to strains of order 10^{-6}.

For glass, this statement corresponds to what one actually sees in the lab, while for steel it is absurd. The reason that energy versus strain in steel does not resemble Figure 3, and that steel does not fail anywhere near the predicted Griffith strains is that thermodynamic arguments are irrelevant. Steel is employed as a structural material precisely because it is impossible for a sharp crack to travel through it with minimal dissipation. Steel, and other tough materials, subject to strains of 10^{-6} cannot reach their thermodynamic ground states.

Thus, one can define a brittle material to be one where a macroscopic sample prepared in the geometry of Figure 1 can be described by Figure 3. Equivalently, restoring force versus displacement is linear to the point of failure. In ideally brittle materials such as glass or silicon, failure occurs when energy per area very nearly equals the minimum thermodynamic energy needed to create new surfaces. In nominally brittle materials, such as Plexiglas (PMMA),

failure occurs at energies well above the thermodynamic minimum, but force versus extension remains linear to the point of failure. This practical definition of brittleness has been employed by experimentalists for many years.

3. Ideal brittle solid

3.1. Definition

This article will focus on a material in which atoms obey the equation of motion

$$m\ddot{\vec{u}}_i = \sum_j \left[\vec{f}(\vec{u}_{ji}) + \beta \vec{g}(\dot{\vec{u}}_{ji}, \vec{u}_{ji}) - b_i \dot{\vec{u}}_i \right]. \tag{11}$$

where $\vec{u}_{ji} \equiv \vec{u}_j - \vec{u}_i$. The atomic motions will be restricted to a plane:

$$\vec{u}_i = (u_i^x, u_i^y). \tag{12}$$

I will work frequently with the *ideal brittle solid* where the functions $\vec{f}$ and $\vec{g}$ have the specific forms

$$\vec{f}(\vec{r}) = \kappa \hat{r}(r - a)\theta(r_c - r) \tag{13a}$$

$$\vec{g}(\dot{\vec{r}}, \vec{r}) = \dot{\vec{r}}\,\theta(r_c - r). \tag{13b}$$

Atoms interact with a central force that varies linearly around an equilibrium spacing of length a, and with force constant κ. If the distance between atoms increases to more than r_c, the force drops abruptly to zero. In addition, atoms experience a dissipative force that is proportional to their relative velocities, and that also drops to zero when the distance between them exceeds r_c. This term, proportional to β, is referred to as *Kelvin dissipation.* Finally, atoms experience a dissipative force proportional to the their velocity; the term proportional to b is *Stokes dissipation*. I will generally allow Stokes dissipation to vary spatially, and in particular set it to zero except near system boundaries.

The force law in Equation (13b) does not determine a unique two-dimensional ground state. The square lattice, triangular lattice, and honeycomb lattice all permit an infinite number of atoms to sit at unit distance from their nearest neighbors. I will focus upon the triangular lattice as the starting point for these studies. The solid formed from the square lattice has undesirable macroscopic properties; it is not isotropic, must be described by three elastic constants, and has a vanishing shear modulus. The triangular lattice and honeycomb lattice are both described by isotropic linear elasticity at large scales, but the triangular lattice is the simpler of the two, and I will focus upon it exclusively from now on.

3.2. Continuum limit

A point which needs to be emphasized is that the theory of atoms described by Equations (11) and (13) *completely contains the theory of isotropic linear elasticity* as a special case. Linear elasticity describes the motion of these atoms when two conditions apply:

1. The relative separations of neighboring atoms minus their original separations are very small compared to the lattice spacing a.
2. The spatial scale characterizing motions of atoms away from their original locations is much larger than the lattice spacing a.

The elastic properties of the solid are given by longitudinal, shear, and Rayleigh wave speeds, which in terms of parameters in Equation (13) are

$$c_l = \sqrt{\frac{9\kappa a^2}{8m}} = 1.06\sqrt{\frac{\kappa a^2}{m}} \tag{14a}$$

$$c_s = \sqrt{\frac{3\kappa a^2}{8m}} = 0.612\sqrt{\frac{\kappa a^2}{m}} \tag{14b}$$

$$c_R = 0.563\sqrt{\frac{\kappa a^2}{m}}. \tag{14c}$$

Equivalently, one can describe the elastic theory through the Lamé constants λ and μ, or Young's modulus Y and Poisson's ratio ν:

$$\lambda = \mu = \frac{\sqrt{3}}{2}\frac{\kappa}{a};\ Y = \frac{5\sqrt{3}}{4}\frac{\kappa}{a};\ \nu = \frac{1}{4}. \tag{15}$$

To form the correspondence with continuum elasticity, the two-dimensional crystal is viewed as a plate of thickness a. It cannot contract in the through-plane direction, and should be interpreted as a plate in plane strain.

In what follows I will treat the two-dimensional brittle crystal as an *experimental material* within which to test concepts in fracture mechanics. This particular experimental material can easily be created on the computer, and probably cannot be created in the laboratory. In the laboratory, a very brittle free-standing film one atom thick would be exceedingly difficult to create. In addition, the forces in Equation (13) while not qualitatively unrealistic are too simple to describe any existing solid quantitatively. On the other hand, there is no reason that the prescriptions of fracture mechanics should not apply as completely to this solid as to any that can actually be realized in the laboratory. The most unrealistic feature is probably the fact that the solid is only one atom thick. Therefore, any phenomena resulting from three-dimensional twisting of a crack line will be lost. There is nothing in the force laws to preclude three-dimensional studies. However, it should be noted that there does not exist any three-dimensional crystal with two-body central forces that reproduces three-dimensional isotropic elasticity in all directions.

3.3. Griffith point

It is simple to use the geometry of Section 2.2 to find the Griffith point for an ideal brittle crystal N rows high, as shown in Figure 8.

Bonds snap when they are stretched beyond their original length by $r_c - a$, so the minimum energy needed per length to permit crack advance (the Griffith energy) is

$$2(\text{two bonds per node}) \times \frac{1}{2} \times \kappa(r_c - a)^2 = \kappa(r_c - a)^2. \tag{16}$$

There are $N - 1$ rows of bonds. When each of them is stretched vertically by a small distance ϵ_y, the length of the bond increases to linear order by an amount

$$r + \epsilon_r = \sqrt{1/4 + (\sqrt{3}/2 + \epsilon_y)^2} \tag{17}$$

$$\Rightarrow \epsilon_r = \frac{\sqrt{3}}{2}\epsilon_y. \tag{18}$$

Therefore, at the Griffith point, the total energy stored per unit length is

$$2(\text{two bonds per site}) \times (N-1) \times \frac{1}{2} \times \kappa(\epsilon_r)^2 = \kappa(r_c - a)^2. \tag{19}$$

$$\Rightarrow \epsilon_r = (r_c - a)/\sqrt{N-1} \Rightarrow \epsilon_y = \frac{2}{\sqrt{3}}(r_c - a)/\sqrt{N-1} \tag{20}$$

If each bond extends vertically by ϵ_y, then at the Griffith point the top of the system extends a vertical distance δ_{yc}

$$\delta_{yc} = \frac{2}{\sqrt{3}}(r_c - a)\sqrt{N-1}. \tag{21}$$

The most important variable in the discussion that follows is

$$\Delta \equiv \frac{\delta_y}{\delta_{yc}}. \tag{22a}$$

That is, Δ is proportional to the strain applied far ahead of the crack, scaled to equal 1 at the Griffith point. The variable Δ can more generally be defined as the ratio between the stress intensity factor at the crack tip to the critical stress intensity factor,

$$\Delta \equiv \frac{K}{K_c}, \tag{22b}$$

where K is chosen appropriately depending upon the mode of loading.

3.4. Analytically solvable case

One of the great advantages of the ideal brittle solid is that there are exact analytical descriptions of crack motion in the limit $r_c \to a$. The solutions make it possible to answer conceptual questions that are difficult to resolve in any other way, and provide guidance on how to construct numerical calculations that can answer a broad array of detailed questions. In particular, the analytical expressions explain how to extrapolate from brief calculations in relatively small finite systems to the macroscopic limit in space and time. That is, they show how one can compute crack properties in a system that might be a few hundred or a few thousand atoms high, over times sufficient for the crack to move a few thousand lattice spacings, and make predictions for crack motions over centimeters in systems that are a billion atoms high. They make this extrapolation possible because the analytical computations are feasible for systems of arbitrary height, and let one compare explicitly results in systems of height 100 and height 10^9 (Gerde, 2001).

The reason that analytical solution is restricted to the limit $r_c \to a$ is that the analytical methods require that the force be a linear function of all particle coordinates, apart from the nonlinearity introduced by the Heaviside θ function. Consider, for example, the particles 1 and 2 originally located at (0,0) and (1,0). Suppose that particle 1 remains at the origin, but particle 2 is displaced by an amount $\vec{u}$. Then the force on particle 1 is

$$\vec{f} = \frac{\hat{x} + \vec{u}}{|\hat{x} + \vec{u}|}[\sqrt{(a+u_x)^2 + u_y^2} - a]\theta(\sqrt{(a+u_x)^2 + u_y^2} - r_c). \tag{23}$$

When r_c is sufficiently close to 1, only very small displacements $\vec{u}$ need to be considered and to leading order the force takes the form

$$\vec{f} = \hat{x} u_x \theta(a + u_x - r_c). \tag{24}$$

Only in the limit where this approximation is valid is the problem analytically tractable.

3.5. WIENER-HOPF TECHNIQUE

The use of the Wiener–Hopf technique for solving lattice models of fracture has been discussed thoroughly in many sources, and I will not go into details of the solutions (Slepyan, 1981, Slepyan, 2002, Marder and Gross 1995, Heizler et al., 2002), but just summarize some results.

In order to make analytical progress, it is necessary to assume that cracks move in *steady state.* This means that if one has two atoms i and j such that in the undeformed crystal

$$\vec{u}_i = \vec{u}_j + n\,a\,\hat{x}, \tag{25}$$

then

$$\vec{u}_i(t) = \vec{u}_j(t - na/v). \tag{26}$$

Thus, if two atoms lie on the same horizontal line in the direction of crack motion, then the time behavior of the two is identical except for a time delay because the crack passes the the left-most atom first. When solutions have this symmetry it is possible to define crack velocity v rigorously in a crystal.

The Wiener–Hopf analysis also involves the dimensionless measure of system loading, Δ, and provides a relation between Δ and the crack velocity v:

$$\Delta = \exp[-\int \frac{d\omega'}{2\pi}\frac{1}{2i\omega'}\left\{\ln Q(\omega', v) - \overline{\ln Q(\omega', v)}\right\}]. \tag{27}$$

All the information about the structure of the lattice and the velocity of the crack is contained in the function $Q(\omega, v)$.

There are several simplified models that contain most features of the full Mode I problem, but for which the algebra is much simpler. The most elementary is a *one-dimensional model* of atomic fracture described by the equations

$$\ddot{u}_i = \begin{cases} u_{i+1} - 2u_i + u_{i-1} & \text{Elastic coupling to neighbors} \\ +\frac{1}{N}(U_N - u_i) & \text{Driven by displacing edges of strip} \\ -2u_i\theta(r_c - u_i) & \text{Bonds which snap} \\ -b\dot{u}_i & \text{Stokes Dissipation.} \end{cases} \tag{28}$$

For this model

$$Q(\omega, v) = \frac{\omega^2 + 2(\cos\omega/v - 1) - 1/N + i\omega b}{\omega^2 + 2(\cos\omega/v - 1) - 1/N + i\omega b - 2}. \tag{29}$$

A model of intermediate difficulty is a Mode III triangular lattice with an even number N of rows of atoms, described by

$$\ddot{u}_i = -b\dot{u}_i + \sum_j f(u_j - u_i), \tag{30a}$$

with

$$f(r) = r\theta(r_c - r). \tag{30b}$$

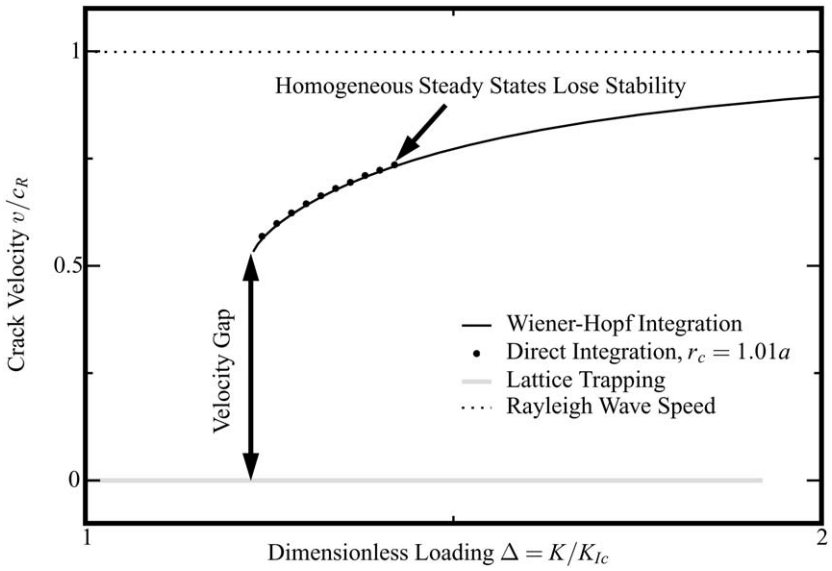

Figure 4. Relation between v and Δ for crack in ideal brittle lattice 20 rows high and Kelvin damping constant $\beta = 0.01$. The exact solution by the Wiener–Hopf technique is compared with solutions of the equations of motion for $r_c = 1.01a$. The diagram illustrates lattice trapping, the velocity gap, a Δ-v relation, and crack instability.

Here u_i is a scalar that can be interpreted as describing motions of atoms perpendicular to the plane in which they lie. Now the solution is given by

$$Q(\omega, v) = \frac{F(\omega, v)}{F(\omega, v) - 1 - \cos(\omega/2v)} \tag{31a}$$

$$F(\omega, v) = \left\{ \frac{y^{[N/2-2]} - y^{-[N/2-2]}}{y^{N/2} - y^{-N/2}} - 2z \right\} \cos(\omega/2v) + 1 \tag{31b}$$

and

$$y = z + \sqrt{z^2 - 1}, \text{ with } z = \frac{3 - \cos(\omega/v) - \omega^2 - ib\omega}{2\cos(\omega/2v)}. \tag{31c}$$

For the Mode I triangular lattice described by Equation (11) and Figure 8, the corresponding expression for Q is so long that it is not useful to record.

3.6. Results from analytical solutions

Figure 4 displays a characteristic result from finding steady states for cracks in the ideal brittle lattice in the limit $r_c \to a$, compared with direct numerical solution of the equations of motion with $r_c = 1.01a$. Analytically one can demonstrate that steady states are stable solutions of the equations of motion (Marder and Gross, 1995), but comparison with direct numerical solution is also valuable because it demonstrates that the steady states really are dynamical attractors for a range of initial conditions. The analytical results exhibit some general features that deserve separate discussion.

3.6.1. *Lattice trapping*

Lattice trapping was first discovered by Thomson, Hsieh, and Rana (1971); subsequent developments are reviewed by Thomson in (1986). The basic idea is that a crack tip in a crystal can be trapped between atoms. Enough energy is stored far enough ahead to make it possible for the crack to advance, but at the same time a static crack is metastable. Atoms just ahead of the crack tip are not pulled far enough from each other for the bonds between them to snap. This is possible for a system above the Griffith point because the Griffith point concerns energy stored per length far ahead of the tip, while lattice trapping concerns forces right in the vicinity of the tip.

The *lattice trapping region* is the range of values of Δ (or G) above the Griffith point for which static cracks are possible because of lattice trapping. For the one-dimensional model of Equation (28) it is easy to calculate (Marder and Gross 1995) that lattice-trapped cracks are stable in the range

$$(\sqrt{3}-1)/\sqrt{2} < \Delta < (\sqrt{3}+1)/\sqrt{2}. \tag{32}$$

3.6.2. *Upper and lower limits on size of lattice trapping*

Temporarily leaving behind the ideal brittle solid, and freely changing the force f in Equation (11), one can ask if there are limits on how large or small the lattice trapping effect can be. There are no limits.

Lattice-trapping can be made as large as one pleases. To make it large, take the interatomic force f to have the forms given in Figure 5(A). The energy contained in the peak can be made as small as desired, but the force needed to overcome it can be arbitrarily large.

On the other hand, lattice-trapping can be made as small as one pleases. For negligible lattice trapping, one can for example adopt for f a force of the form illustrated in Figure 5(B). Almost all the energy needed to break bonds must be spent in the region where the force is constant. Figure 5(C) provides a sketch of atomic positions for one-dimensional model Equation (28) where the force has the form shown in Figure 5(B). The crack tip divide into three regions, a left-hand region where the force between horizontal lines of atoms has vanished, a middle region where the force is constant, and a right-hand region where the force is linear. In the limit where l_c is large, one finds that the middle region has approximately length p where

$$p \approx \frac{\Delta + \sqrt{\Delta^2 - 1}}{\sqrt{2}} \sqrt{l_c / l_0}. \tag{33}$$

Lattice trapping ends when the distance between the atoms at position 1 rises above distance l_0, and is given by

$$\Delta = 1 + \sqrt{\frac{l_0}{2l_c}}. \tag{34}$$

Thus in this case, by making l_c/l_0 large, the domain of lattice trapping can be made as small as desired.

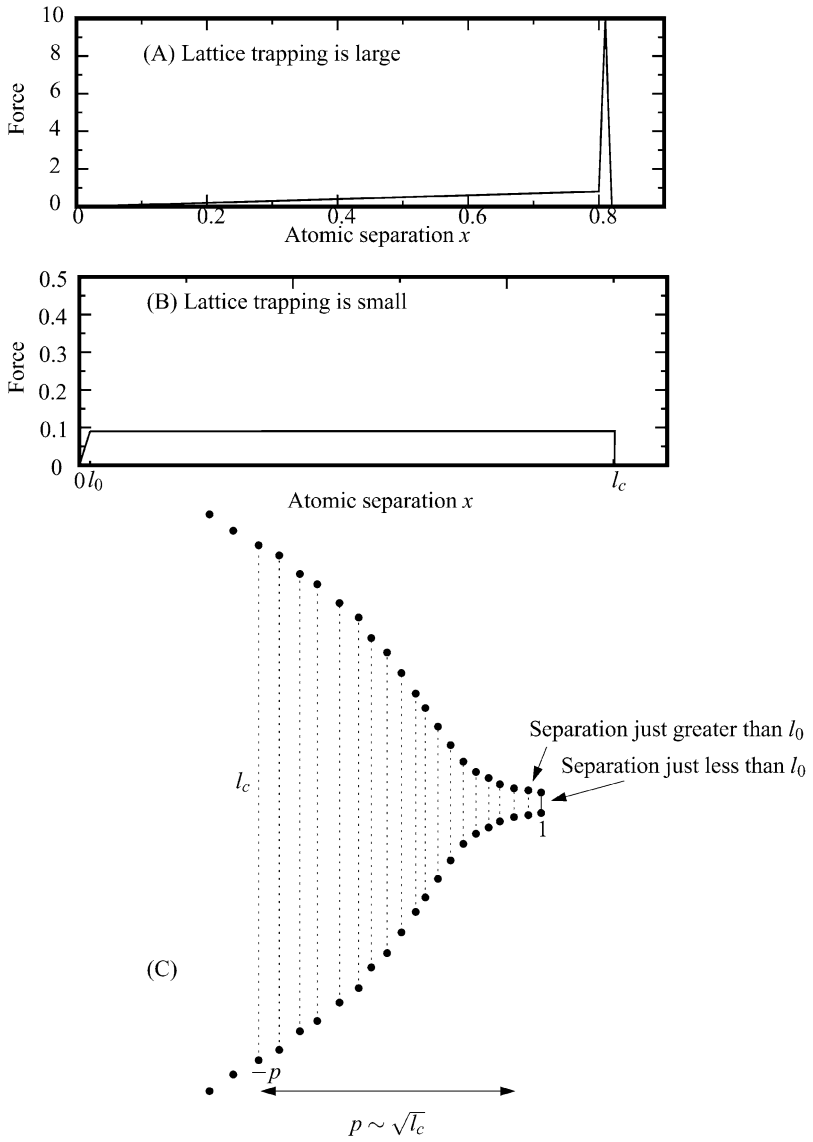

Figure 5. (A) Interatomic force law that would lead to very large lattice trapping region. (B) Interatomic force law that would lead to very small lattice trapping region. (C) Configuration of atoms around crack tip corresponding to weak lattice trapping.

3.6.3. *Velocity gap*

The velocity gap was first noted by Marder and Liu (1993). It is a dynamical analog of lattice trapping. There is a forbidden range of velocities for steady-state cracks in crystals at zero temperature. Either cracks are stationary, or else they run at a substantial fraction of the shear wave speed, usually 30% or more.

The velocity gap emerges from detailed solutions for crack motion, and from molecular dynamics studies of many different models, but it is helpful to have a qualitative argument explaining how it arises.

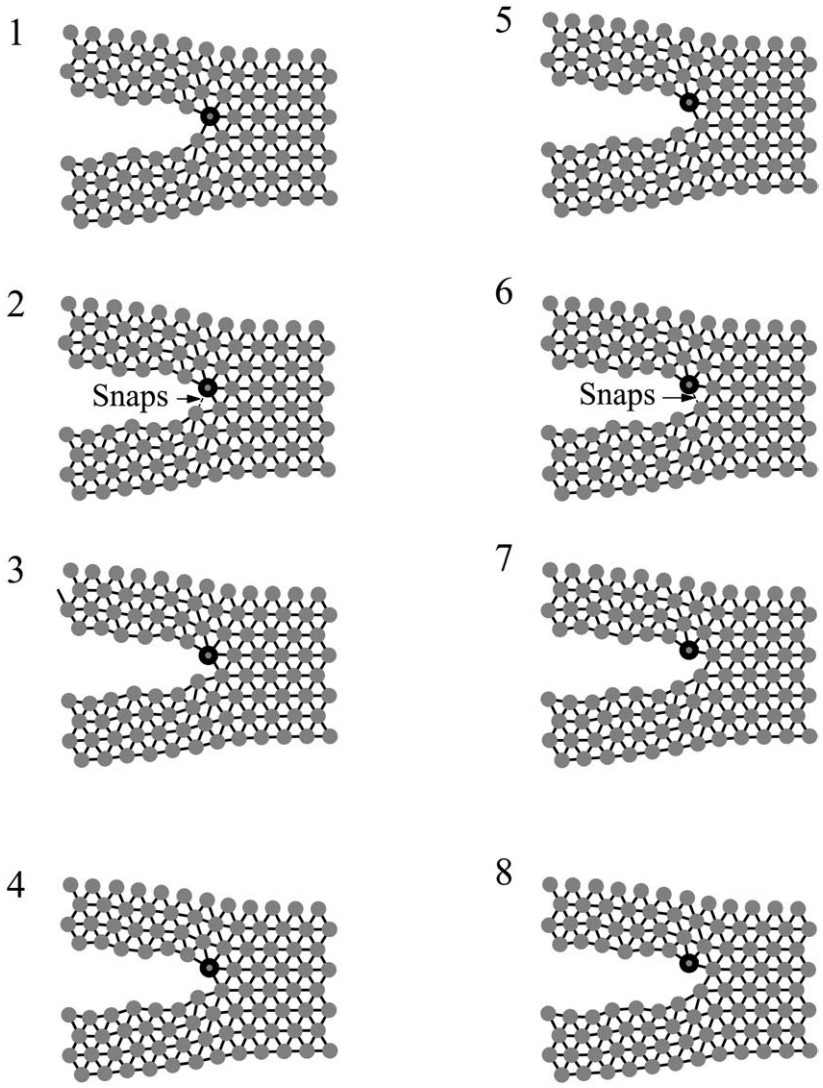

Figure 6. Sequence of eight snapshots from motion of a crack tip. Bonds break in frames two and six. The circled atom snaps backward each time a bond connected to it breaks, providing a crucial portion of the energy for the next bond to snap. This process must occur within the first half of the first vibrational period of the encircled atom, or it is unlikely ever to occur.

Dynamic fracture is a cascade of bonds breaking, one giving way after another like a toppling line of dominoes. Examining Figure 6, watch what happens as a crack moves ahead. In frame 2, the bond between two atoms has just broken. There is no guarantee that the next bond to the right will break. The crack could fall into a static lattice trapped state. The only way to avoid this fate is for the circled atom to deliver enough of an impulse to its right-hand neighbor that the bond on that neighbor is broken in turn. This process had better take place within the first half of the first vibrational period of the circled atom. The longer it vibrates, the more energy will be distributed to its neighbors in all directions in the form of traveling waves, and the smaller become the chances that there will be enough concentrated energy available to snap the next bond down the line.

To make this idea slightly more quantitative, let $\mathcal{K}_b$ be the *effective* spring constant acting on an atom after a bond connected to it has snapped. Its oscillatory period is

$$\tau = 2\pi\sqrt{\frac{M}{\mathcal{K}_b}}, \tag{35}$$

where M is its mass. Assuming that the next bond, at distance a, breaks during some fraction $\alpha < 1$ of half this oscillatory period, the speed v of the crack will be

$$v = \frac{a}{\alpha\pi}\sqrt{\frac{\mathcal{K}_b}{M}}. \tag{36}$$

By this same rough logic, the speed of sound is given by solving the wave equation

$$M\ddot{u} = \mathcal{K}a^2\frac{\partial^2 u}{\partial x^2}, \tag{37}$$

where now $\mathcal{K}$ is an effective spring constant appropriate for atoms surrounded by unbroken bonds. From Equation (37) follows a wave speed c of

$$c = a\sqrt{\frac{\mathcal{K}}{M}} \Rightarrow \frac{v}{c} \geq \frac{\alpha}{\pi}\sqrt{\frac{\mathcal{K}_b}{\mathcal{K}}}. \tag{38}$$

Even from these rough arguments, one should expect v/c to be less than one. When one of the springs connected to an atom is snapped, the effective spring constant describing its vibrations should decrease, so $\mathcal{K} > \mathcal{K}_b$. In addition, $\alpha < 1$, and finally there is a factor of π in the denominator of Equation (38), reducing it still further.

The crack speed v estimated here is a lower bound. There is no way that pulling more gently on remote system boundaries can reduce the vibrational period of two atoms once the bond connecting them breaks. Pulling harder on external boundaries can however increase the speed of a crack because it can supply enough energy that the atoms are already moving quickly when the bond between them snaps.

These arguments presume that the only source of energy available for snapping bonds is contained in strained material ahead of the tip. This assumption is never completely correct. At any nonzero temperature, thermal fluctuations can bring extra energy in. For this reason, cracks strained above the Griffith point at $\Delta = 1$ always move ahead at any nonzero temperature, but the rate is very small when the thermal fluctuations are rare. Similarly, chemical agents in the environment can help catalyze bond breaking, and crack speeds are sometimes controlled by the rate at which they arrive. Thus, one should expect the velocity gap to disappear in any crystal as the temperature increases, or as crack motion becomes dominated by chemical processes. This expectation is borne out in molecular dynamics studies (Holland and Marder, 1999).

An additional idea suggested by the existence of lattice trapping and the velocity gap is *irreducible dissipation*. One would like to be able to cleave a solid slowly enough that the energy needed to make new surfaces approaches the surface energy. For a solid where the relation between crack velocity and loading has the form shown in Figure 4, this goal is practically impossible to achieve. The crack motions on the adiabatic branch of the curve do indeed allow cleavage with no more energy consumption than the thermodynamic minimum. However, the velocities are so low that they are experimentally inaccessible. To arrive at velocities that could

separate a centimeter-long crystal on timescales of a second, one has to move up to values of Δ where dissipation consumes on the order of half the fracture energy. Essentially, because the crack either moves fast or does not move at all, it cannot move without dissipating energy, and attempts to make it move slowly result in a succession of rapid dissipative events.

3.6.4. *Instability*

In order for the solutions given by Equation (27) to be correct in a homogeneous solid, bonds along the crack line must break in sequence, and atoms along the crack line must be the only atoms for which it is ever true of nearest neighbors that $u_{ij} > r_c$. The analytical solutions make it possible to check when this condition is obeyed. Once Δ exceeds a critical value Δ_c, horizontal bonds above the crack line vibrate with sufficient amplitude that they violate this condition at some point during the passage of the crack tip.

What happens as a result for $\Delta > \Delta_c$ depends upon many details of the physical model. One could decide that the bonds along the crack line are in fact weaker than those elsewhere, in which case the analytical solutions could continue to apply. In a homogeneous material, the tip may blunt, and emit transverse microcracks or dislocations.

3.6.5. *Scaling laws*

One of the most important ideas to emerge from Wiener–Hopf solutions of ideal brittle systems is that when expressed in terms of the correct variables, the relation between velocity v and dimensionless strain Δ becomes independent of system height for very small systems. This statement is particularly accurate for the models accessible by the Wiener–Hopf technique, as shown in Figure 7. The calculations are carried out for strips of height 20 through 160, and with Kelvin damping of magnitude $\beta = 0.01$. At the lower end of the velocity range changes in the curves are imperceptible. A strip of height 20 reaches a velocity of $v/c_R = 0.53$ for $\Delta = 1.2280$, while a strip of height 160 reaches the same velocity for $\Delta = 1.2284$.

The velocity curves in Figure 7 are displayed extending up to large values of Δ. As discussed in the previous section, a crack in an homogeneous brittle medium should become unstable before reaching such large values of Δ. However the curves are not completely meaningless. It is possible both experimentally and numerically to prepare cracks that travel along weakened interfaces, so that instabilities taking the crack tip off the crack line are suppressed Washabaugh and Knauss, 1994). Thus, such curves could in principle be measured.

The velocity curves begin to diverge from each other noticeably only as they approach the Rayleigh wave speed c_R. In conventional fracture mechanics, Mode I cracks cannot exceed the Rayleigh wave speed. As one sees from Figure 7 this restriction is a macroscopic phenomenon. In small systems where instabilities have been suppressed, crack speeds pass continuously through c_R and increase. As the height of the system increases, a plateau develops in the v-Δ relation and Δ must increase to larger and larger values in order to raise the crack above the Rayleigh wave speed. As the system height increases to infinity, the plateau becomes infinite in extent and infinite energy is required for crack motion at the Rayleigh wave speed.

In any given physical situation, one must ask whether height independence of the v-Δ relation is reasonable. It is reasonable only if the system is much larger than the region in which energy is dissipated. With Kelvin dissipation, this scale is reached almost immediately, while for Stokes dissipation it can never be reached (Figure 12). In more complex numerical or experimental systems, one must ask about the size of the process zone, and can only draw the simple conclusion that v-Δ is independent of system size when the process zone is much smaller than the system.

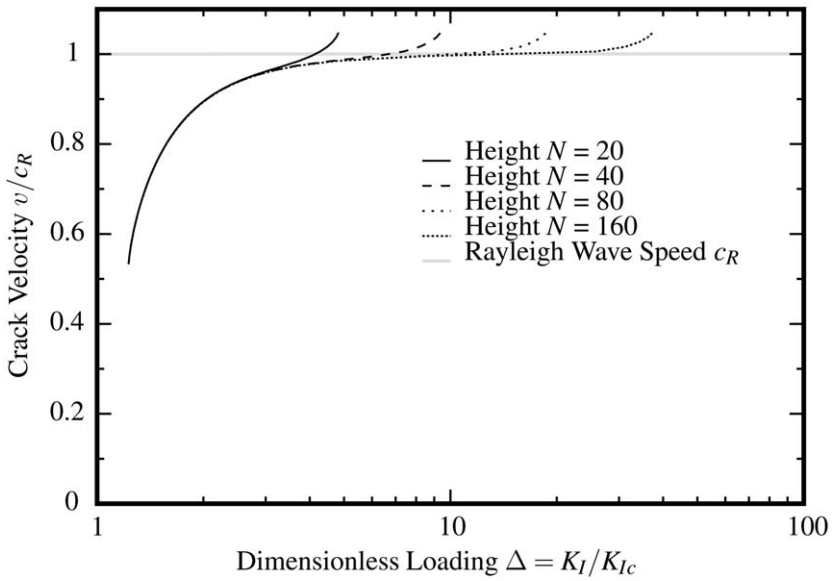

Figure 7. Relationship between velocity v and dimensionless strain $\Delta = K_I/K_{Ic}$ for Mode I lattice strips of varying height. The calculations are performed with Kelvin dissipation $\beta = 0.01$. The left-hand portions of the curve are almost completely independent of system height. The cracks are presumed to travel along a weak interface that precludes transverse instabilities, and therefore the curves continue up and through the Rayleigh wave speed. Were the curves to be terminated at the points where cracks become unstable in homogeneous crystals, they would be nearly indistinguishable.

3.7. Laboratory significance of atomic-scale results

It is not immediately clear what significance to give to solutions of the atomic-scale models. Different aspects of the solutions are likely to have different degrees of relevance to laboratory experiments.

3.7.1. *Lattice trapping*

Lattice trapping describes the prediction that atomically sharp cracks can be trapped by a lattice under conditions of remote loading when enough energy is present for them to run. This phenomenon is familiar experimentally, and corresponds to the fact that the stress intensity factor K_{Id} at which cracks begin to run dynamically is generally greater than a range of stress intensity factors K_I for which rapid motion is possible. However, the limit of lattice trapping calculated theoretically is likely to provide neither an upper bound nor a lower bound for the experimental value of K_{Id}. In a sample at a temperature of $T = 0$K and loaded infinitely slowly, lattice trapping would provide a lower bound on K_{Id}. No crack would begin to run until the value of K_I provided by lattice trapping was exceeded. However, the presence of any sort of noise or vibration, whether due to temperature or acoustic waves in the laboratory, can shake a crack loose before the stress intensity has reached this threshold. In practice, cracks should be able to run before the lattice trapping limit has been exceeded. On the other hand, the lattice trapping limit does not have to correspond to an upper bound on crack initiation either. Crack tips can be trapped by kinks, by impurities, by dislocations, and by voids or other blunting configurations. All of these trapping mechanisms present higher energy barriers to crack motion than lattice trapping. No one has yet made the case for any material that the

practical problem of initiating a crack can reasonably be treated by calculating the limits of lattice trapping.

Lattice trapping only exists, technically speaking, at zero temperature. At any nonzero temperature, thermal fluctuations must always allow a crack above the Griffith threshold to creep ahead at some rate. The rate was calculated for some simple cases by Marder (1996). The rate will generally be proportional to $\exp[-\delta U(\Delta)/k_B T]$, where $\delta U(\Delta)$ is the energy needed to pull a bond from its location in a trapped state to the breaking point.

3.7.2. *Velocity gap*

The velocity gap describes the inability of a crack moving steadily under conditions of constant stress intensity factor to travel at less than lower critical speed. It is entirely possible that this predication will be borne out in laboratory experiments, although a conclusive demonstration has not yet been provided. The lowest Δ at which cracks can run sometimes may provide the value of K_{Ia}, the stress intensity factor at which laboratory cracks arrest. However, this statement will only be true at temperatures low enough that thermal creep of cracks can be neglected. There is good experimental evidence that typical brittle materials, both amorphous and crystalline, do not display a velocity gap at room temperature (Hauch and Marder, 1998, Holland and Marder 1999). The theoretical explanation is that thermal fluctuations are large enough at room temperature for cracks to run at any speed. The best current estimates are that the velocity gap might be observed in single-crystal silicon at temperatures below 100 K. At room temperature, the calculations leading to the velocity gap may still provide a good estimate of K_{Ia}, but this has never been checked carefully. The general experience of experimentalists is that rapidly traveling cracks tend to decelerate very rapidly and somewhat unpredictably to rest. Thus, while no velocity gap exists at room temperature, the mental picture it provides of a hysteretic separation between rapidly moving and static cracks is more realistic than the continuous relations between K and v that theorists are prone to assume.

3.7.3. *Velocity versus loading relations*

The quantity of greatest potential experimental significance is the computed curve $\Delta(v) = K_I(v)/K_{Ic}$. In this computation, a perfectly straight crack front runs through a perfect material breaking the absolute minimum number of atomic bonds. It is difficult to believe that an experimental crack could find a way to traverse a material at the same speed while spending less energy. Therefore, for any given velocity v, $\Delta(v)$ plausibly provides the minimum stress intensity factor or energy release needed for crack motion. The most careful attempt so far to check this assertion provides evidence that contradicts it; experiments in single crystals of silicon show cracks traveling with values of Δ smaller than those required in molecular dynamics simulations (Holland and Marder, 1999, Swadener et al. 2002). Nevertheless, it is difficult to see where the argument goes wrong, and either the experiments or the molecular dynamics simulations need to be re-calibrated.

3.7.4. *Instabilities*

Yoffe's goal, in the first detailed theoretical paper on dynamic crack motion, was to predict the onset of branching (Yoffe, 1951). Perfectly steady crack motion becomes unstable for $\Delta > \Delta_c$, signaling the start of a progression of instabilities that leads ultimately to crack branching. However, one cannot identify Δ_c with the stress intensity factor that produces branched cracks. For Δ not much larger than Δ_c, crack solutions may deviate from perfect straightness on the scale of only a few atoms. Such small imperfections would at best be visible

if a crack surface were examined after the fact through atomic force microscopy, and cannot be identified with the phenomenon of branching, which leads to two or more macroscopic cracks.

3.8. Macroscopic equations of motion

A point that deserves some emphasis is that if the relation between loading Δ and crack velocity v is obtained from microscopic calculations, then one is immediately in possession of a macroscopic equation of motion for cracks in arbitrary geometries. Finite element calculations involving cracks in plates determine the stress intensity factors K_I and K_{II} surrounding the crack tip. Assuming the principle of local symmetry (Goldstein and Salganik, 1974, Oleaga, 2001), the crack tip will move in the unique direction such that $K_{II} = 0$, and at the speed given by inverting $K_I/K_{Ic} = \Delta(v)$. If some other principle to determine crack direction based upon K_I and K_{II} were obtained, that could be used as well. So far as macroscopic fracture mechanics is concerned, microscopic calculations provide a look-up table describing how crack tips respond to external loading conditions.

4. Numerical solutions of finite systems

4.1. Significance of scaling

As soon as the interatomic force laws deviate from the form in Equation (13) in the limit $r_c \to a$, neither are analytical expressions such as Equation (27) any longer available, nor have reliable analytical approximations been found to replace them. However, scaling results such as those in Figure 7 point to numerical procedures that make it possible to arrive at macroscopic predictions for very general interatomic potentials.

There are two hypotheses that make it possible to derive macroscopic predictions from microscopic calculations.

1. *Cracks reach steady states.* In crystals in the thin strip loading configuration, the hypothesis is that Equation (26) continues to be obeyed exactly. More generally, one may assume that cracks travel in a statistically self-similar manner, and that observing their motion over a small time interval is sufficient to make very long term predictions.
2. *Crack motion is dictated by K or Δ independent of system size.* This conclusion is clearly suggested by Figure 7. However, it is equivalent to one of the central ideas lying at the heart of fracture mechanics. Fracture mechanics asserts that the stress fields around a crack tip adopt a universal character depending only upon the stress intensity factors. Once this field has developed, the crack tip has no way to know whether it is sitting inside a solid 1000 atoms high or 10^{12} atoms high. Once Δ or equivalently K are the same, measuring the response of the crack tip in a small system must be equivalent to measuring its response in the large one. The only surprise from the atomic point of view is that in brittle solids the universal response of cracks to loading sets in with great accuracy in systems so small that the the universal $1/\sqrt{r}$ stress fields do not have room to establish themselves.

Thus one derives from exact analytical solutions the expectation that by searching for steady states in small systems, one can make predictions about the long-time behavior of cracks in macroscopic samples. The success of this procedure, at least in its simplest form, requires that the material be very brittle, so that there are no active structures on length

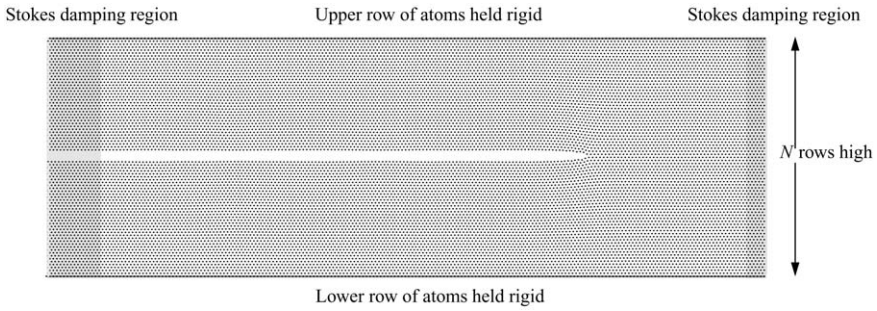

Figure 8. Configuration of numerical experiment to find steady crack states for Figure 9. Atoms are originally arrayed in a triangular lattice 80 rows high, and three times as long as it is tall. Top and bottom rows of atoms are separated vertically by the distance y_c given in Equation (21) and held rigid. The crack tip is defined as the location of the rightmost atom whose nearest vertical neighbor is at distance greater than $2.5a$. When the crack tip approaches within $60a$ of the right boundary, 10 columns of new crystal are attached to the right boundary, and the same amount discarded from the left hand side.

scales between the atomic and macroscopic. I now turn to a detailed description of how the computations can be conducted.

4.2. Details of numerical solution

Scaling solutions have been obtained for cracks in numerical materials with rather complicated interatomic potentials (Holland and Marder, 1999). However, the ideas are better illustrated through the simple model systems that are the subject of this paper. I will discuss the computations needed to find the relationship between crack speed and loading Δ in a strip 20 rows high with $r_c = 1.01$. Results of such runs appear in Figure 4. The geometry needed for such runs is illustrated in Figure 8. However, this figure shows atomic positions from one of the runs used in creating Figure 9 where $r_c = 1.2$, since atomic motions are so small when $r_c = 1.01$ that the eye has trouble picking out the existence of a crack.

Computations for Figure 4 were performed for a triangular lattice 20 rows high, with $r_c = 1.01a$, and $\beta = .01\kappa$. In the limit $r_c \to a$, it is necessary to put some damping into the model if one wants to have brittle fracture. This sounds a little paradoxical, since it means that the model is more brittle with some damping than without it. Without any damping, the range of Δ above the lower end of the velocity gap and below the microcracking instability closes down to zero, and there are no stable steady crack solutions. A small amount of Kelvin damping prevents atoms from vibrating so much near the tip that they cause it to blunt, and permits a range of brittle solutions.

To find the relation between v and Δ through direct integration of equations of motion, one follows these steps:

1. Create a crystal with N vertical rows and length l. For the particular purpose of comparing with Figure 4, choose $N = 20$, leading to a height $h = 16.45$ and length $l = 3h$. The decision to use an aspect ratio of 3:1 is based upon numerical experiments in which the aspect ratio was varied. At an aspect ratio of 2:1, some effects of the boundaries were still visible, altering the velocity on the order of 10%, while increasing the aspect ratio from 3:1 to 4:1 produced no change in numerically measured velocities to one part in a thousand.
2. Find the Griffith energy. To do so, calculate the potential energy of the crystal in its ground state. Next, move all atoms above the center line vertically upward a distance larger than

r_c and compute the total energy of the system again. Dividing by the length of the system gives the Griffith energy. In the present case, $E_G = 10^{-4}$.

3. Find the Griffith strain. To do so, uniformly strain the system in the vertical direction, measuring the potential energy after each small increment; in this case, an additional 0.5% above its original height in 100 increments. Monitor the total potential energy of the system divided by system length. As soon as this quantity exceeds the Griffith energy, as computed in the preceding step, use interpolation to find the strain at which the potential energy per length equals the Griffith energy, as in Figure 2. Note that this computation does not presume that the strain energy has the quadratic form of Equation (6). For the case of $r_c = 1.01$, the Griffith strain is $e_{yy} = 3.06 \cdot 10^{-3}$.
4. Based upon inspection of Figure 4, one expects moving states to begin around a value of $\Delta = 1.23$. It is very difficult to initiate moving cracks from rest right at the lowest values of Δ where they can occur, so choose $\Delta = 1.32$, and uniformly strain the crystal up to $e_{yy} = 3.06 \cdot 10^{-3} \times 1.32$.
5. As an initial condition, put atoms in a crack-like configuration. At the left side of the sample, there is an open space between two portions of crystal, separated along the center line. The height of the open space is precisely he_{yy}; above and below the opening there is unstrained equilibrium crystal. Moving horizontally toward the center of the crystal, the crack faces come together, until at some point near the center they close up. Further to the right there is uniformly strained crystal. One could go to some lengths to have atomic locations around the seed crack that are in accord with results for continuum elastic fields around a crack tip, but I know of no gain for going to this effort. Instead, set all atoms' velocities to zero, set the coefficient of Stokes damping b to 0.2 everywhere in the crystal, and allow the system to evolve dynamically for 1000 time steps. The crack is lattice trapped, and because of the presence of Stokes damping atoms simply relax to a metastable static configuration.
6. Retain all atomic positions, set all velocities to zero, and set Stokes damping to zero everywhere except at the system boundaries as shown in Figure 8. These Stokes damping regions are especially important if no other dissipative terms are present, for unless energy emitted by the crack tip dissipates, it will return to the crack tip and destroy it. In an infinitely long strip damping regions are not needed, since instead the radiation created by the tip travels to infinity. In the present case, take $b(x) = (1 - x_r/10)\theta(1 - x_r/10) + (1 - x_l/5)\theta(1 - x_l/5)$ where x_r is the distance (in equilibrium) of an atom from the right hand side of the system, and x_l is its distance from the left hand side of the system. The crack tip should never be allowed to reach the regions where the damping is nonzero.
7. To induce a dynamic state, give vertical velocities to atoms on the crack faces behind the tip. For example, establish a positive vertical velocity of $c_l/100$ for 4 horizontal atoms on the upper crack face behind the tip, and a negative vertical velocity of the same magnitude for 4 atoms on the lower crack face.
8. Remove the atoms along the top and bottom edges of the system from the list of atoms whose positions will be updated dynamically. The top and bottom edges need to be held rigid. One row of atoms suffices.
9. Initiate dynamics. I use the Verlet (1967) algorithm with $dt = .025$. Decreasing the time step by a factor of 2 produces no change in measured velocities to one part in 1000.
10. To study steady state cracks, it is important to be able to cut and paste as the crack runs along. When the crack tip reaches within 75% of the end of the system, displace the entire crack configuration back by 10 unit cells, discarding broken material on the left hand side,

and adding on new strained crystal on the right hand side. In this way, one can obtain crack runs that are many times the apparent length of the atomic system, and without being able to do so it is impossible to obtain accurate measurements of crack velocities.

11. Slightly increment or decrement Δ, moving all atoms so that the top and bottom boundaries are at the new correct locations, and so that the material far to the left of the crack tip is in equilibrium, and far to the right is uniformly strained, but otherwise retaining atomic positions and velocities. By proceeding carefully in this manner, one can map out a broader range of dynamic crack states than is possible by starting with static configurations and kicking atoms along the crack line. In particular, by slowly lowering Δ one can obtain running cracks all the way down to the limit imposed by the velocity gap. To obtain accurate velocities, I vary Δ by 1% in the time it takes sound to run 10 times from the crack tip to the vertical boundary and back.

There are two common errors that can appear in first attempts to perform atomic-scale fracture simulations. The first is to start with a crack configuration that is attracted to a lattice-trapped state and to conclude that dynamic cracks are impossible for those parameters. The second is to choose a system that is too short in the horizontal direction, and with too ineffective a damping region on the right hand side. What happens in this case is that the kinetic energy around the crack tip increases without limit for as long as one runs the simulation until the crack tip breaks apart. Such crack branching is a real physical phenomenon when Δ exceeds the instability threshold, but to conclude that it occurs for all Δ is an error resulting from improper treatment of outgoing waves.

Cracks in ideal brittle solids in the limit $r_c \to a$ can be compared directly with the Wiener–Hopf theory (Figure 4 and Heizler et al., 2002), which has the advantage of providing a careful check both of the numerical procedures and the Wiener–Hopf analysis. However, this limit is not a good one for investigating most physical questions. The cracks are difficult to initiate, survive only over a small range of Δ, and easily blunt and stop. Brittle fracture becomes more robust when the range of interaction is larger. Figure 9 shows the relation between v and Δ when the point at which bonds snap increases to $r_c = 1.2a$. This value is consistent with the range of interatomic interactions in real brittle solids, such as oxide glasses or silicon. It is easy to initiate fractures, and they are stable over a wider range of loads than was the case for $r_c = 1.01a$. There is the disadvantage that Wiener–Hopf solutions are no longer available for comparison. However, having verified carefully at $r_c = 1.01a$ that the numerical procedures are accurate, one can proceed to investigate progressively more realistic models with confidence.

According to Figure 9, for systems of height $N > 40$ and $\Delta > 1.4$, perfectly steady crack motion is no longer stable. In Mode III models, the crack emits small shoots and keeps running (Marder and Liu, 1993). In Mode I, the crack tips blunt and the cracks arrest. The situation is analogous to lattice trapping, but with a blunted crack tip providing a larger trapping barrier .

Studying cracks where bonds break off the main crack line requires some choices in the modeling procedure that have not been discussed until now. These concern choosing the list of particles with which each atom interacts; that is, in Equation (11), the list of particles indexed by j. Taken literally in a system populated by a single species of atom, the only physical choice would be to allow j to range over all atoms in the system, permitting interaction between any two atoms that come within distance r_c of each other. It is numerically very inefficient to perform such a large sum at each time step. A much better procedure, which has the same result, is to divide space into cubic boxes of size r_c, and create a list of all the particles in each box. One can carry out a sum over all particles by running over all boxes, and then summing

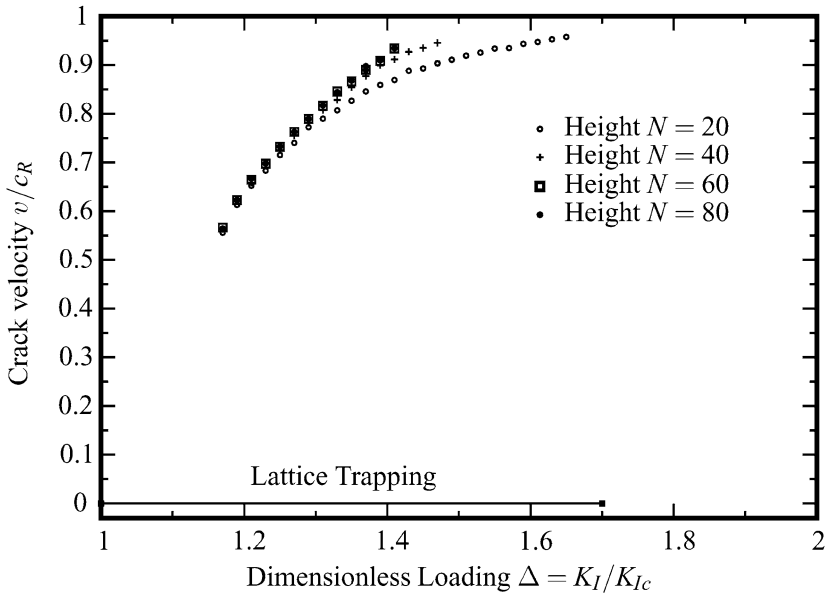

Figure 9. v-Δ diagram for ideal brittle solid with bond-snapping length r_c=1.2 and Kelvin viscosity $\beta = 0.01$. Computations are carried out for lattices 20 to 80 rows high to demonstrate that the results are practically independent of the height N once the number of rows reaches 60.

over all the particles in each box. In searching for neighbors j with which particle i interacts, one just looks in adjoining boxes.

Experiments show that it may be better to treat bond-breaking as an irreversible process. The cause of irreversibility could be that oxides bond to exposed surfaces. Or it could be that degrees of freedom treated as particles in the model are actually complex molecular units with internal degrees of freedom that prevent rejoining once bonds are broken. For the modeling in this paper, I have adopted a rule that neighbors j in Equation (11) are determined from locations in the original undeformed crystal, and if new atoms come within range of particle i as the crystal deforms they do not interact. Because of this choice, when crack tips become unstable, they emit cracks in new directions, but not dislocations. For dislocations to form, it must be possible for atoms that were not originally nearest neighbors to bond together, and I decided not to permit that in the simulations described here.

Figure 11 shows what happens as one proceeds to larger values of Δ. From a value of $\Delta = 2.5$ and higher, the blunted tips that caused crack arrest at $\Delta = 1.4$ are no longer stable, and cracks begin to move again. The motion is now much rougher than before, with irregular crack paths as shown in Figure 10, and sometimes multiple crack tips traveling simultaneously. The crack tip and velocity can no longer be defined as precisely as before. In practice, the rightmost location where two originally neighboring atoms have separated more than a critical vertical amount is identified as the tip.

Despite the considerably less precise nature of crack motion once true steady states are gone, it is still possible to describe a relation between loading Δ and crack front speed v, as displayed in Figure 11.

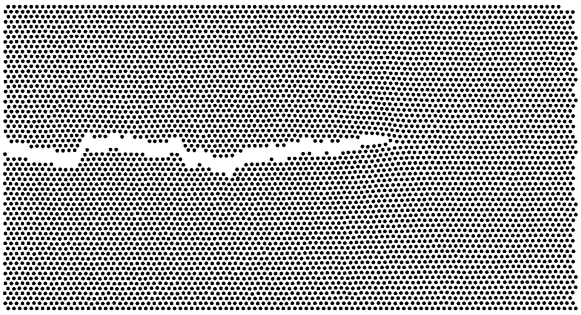

Figure 10. Typical crack path for $\Delta > 2.5$ in system of height $N = 80$.

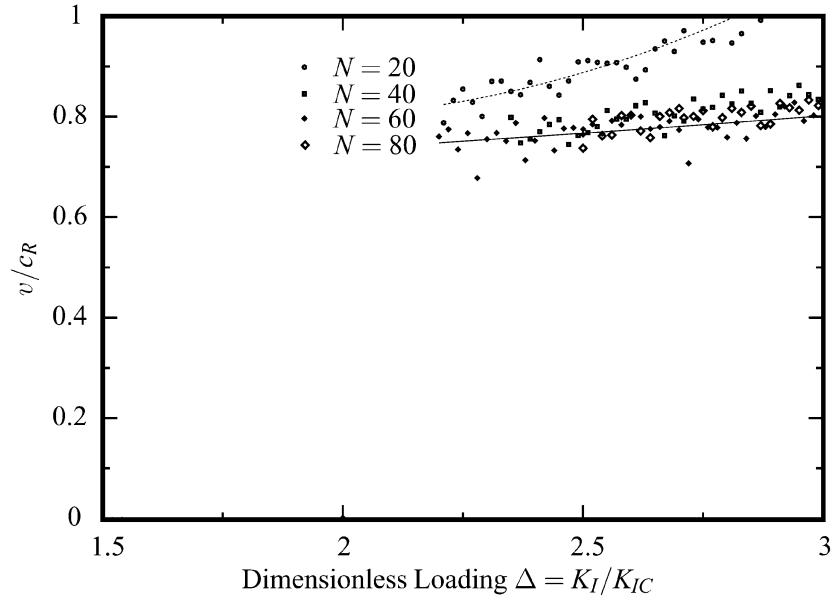

Figure 11. v-Δ diagram for ideal brittle solid with bond-snapping length $r_c = 1.2$ and Kelvin viscosity $\beta = 0.01$. Computations are carried out for lattices between 20 and 80 rows high so as to monitor convergence toward the infinite limit. Now however, the computations are performed for large values of Δ for which the crack travels irregularly and can escape from blunted configurations. The relation between crack speed and loading acquires a statistical character. Two quadratic regression lines are shown; one through the results for $N = 20$ and one for the results for $N = 60$ and $N = 80$.

4.3. Laboratory significance of calculations

It is interesting to ask which of Figure 9 or Figure 11 more likely represents observations that would be made in the laboratory on macroscopic samples. In truth, this question does not yet have a completely clear answer. The problem is not so much that the computations are performed on very small samples, but that they leave out a number of ingredients that inevitably are present in real systems. The list of these ingredients should at least include

- Extension to fully three-dimensional samples.
- Nonzero temperature.
- Misaligned and irregular boundary conditions.
- Imperfections in crystal.

Some of these ingredients will be added to the model in subsequent sections. The general conclusion from the investigations is this:

Perfect steady states in two-dimensional crystals are not robust. Pull them too hard, as shown in Figure 9 and they arrest. Tilt the crystal, even by a degree, and they do not propagate. Permit temperature fluctuations and imperfections, and they arrest. Based upon these observations, it seems that the states such as those shown in Figure 10 and 11 are realistic, while those in Figure 9 are not. However, this conclusion contradicts experiment. Cracks in Figure 11 do not begin to propagate until the energy release is more than 4 times the energy needed to create new surfaces. Laboratory experiments in crystals clearly show cracks propagating at high speeds when the energy available to them is little more than the minimum energy needed for surface creation (Hauch et al., 1999, Spence et al., 1993).

One possible explanation for this observation is that is easier to stop a crack in two dimensions than in three. In two dimensions a single atom out of place can stop a crack. In three dimensions, a single atom out of place will cause a microscopic disruption, but a large part of the crack front may keep moving. Thus it may be that if one wants to perform two-dimensional simulations of three-dimensional cracks, the precisely controlled conditions of Figure 9 are more realistic than they seem at first. However, this issue has not yet been investigated carefully, and is not yet settled.

4.4. Dissipation

The atomic equations of motion in Equation 11 contain two sorts of dissipation, Stokes and Kelvin. These two dissipative terms have very different properties when one thinks about the macroscopic limit.

Stokes dissipation is unphysical unless it arises because of interaction between the atoms and some external agent. Otherwise there is no way to explain why the velocity $\dot{u} = 0$ is special and causes the dissipative force to vanish. If the coefficient of Stokes dissipation is nonzero for all atoms, one should view the sample as being embedded in a gooey dissipative medium. As one proceeds to larger and larger samples, more and more energy will is lost to this medium as the left hand side of the sample behind the crack relaxes to its equilibrium shape. The energy needed to feed this dissipative process eventually completely dominates the energy needed to feed the crack tip. Calculations illustrating this point are contained in Figuare 12. These calculations explain the choice always to set the coefficient of Stokes dissipation to zero except in a narrow strip of material near the end of the sample where it serves to absorb outgoing radiation (Figure 8).

Kelvin dissipation has a very different physical interpretation. It depends upon the relative velocity between neighboring atoms, and therefore makes physical sense even when there is no external heat bath present in the system. In metals, ions are surrounded by electron clouds, and the adjustment of the electrons as the ions move produces dissipation of the Kelvin type (Holian and Ravelo, 1995).

However, from a macroscopic point of view Kelvin dissipation is forbidden, because it leads to infinite energy dissipation in the neighborhood of a crack tip singularity. Therefore, from a macroscopic perspective, Kelvin dissipation cannot coexist with cracks (Willis, 1967).

To demonstrate this claim, note that in a macroscopic description, the energy lost to Kelvin dissipation takes the general form

$$\dot{\mathcal{E}} \sim \int d^2 r \dot{\vec{u}} \cdot \beta \frac{\partial}{\partial t} a^2 \nabla^2 \vec{u}. \tag{39}$$

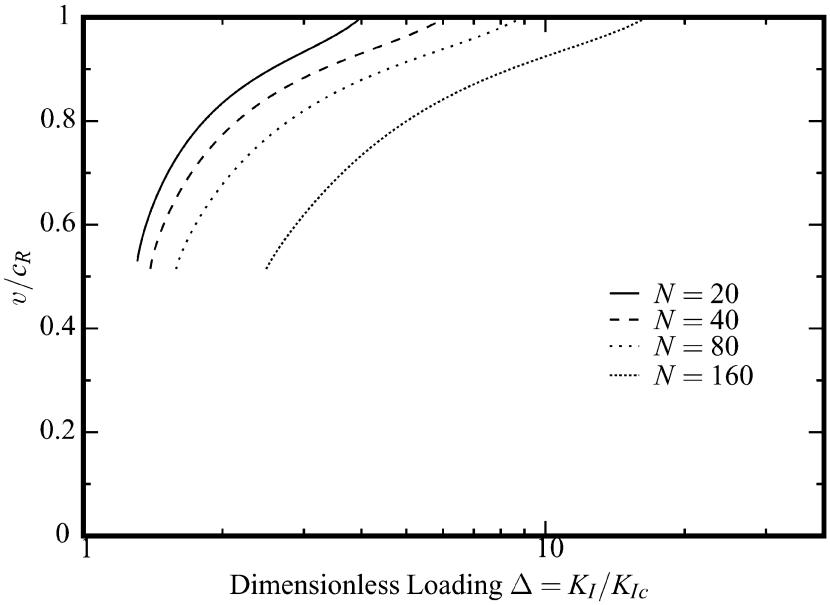

Figure 12. Relationship between velocity v and dimensionless strain $\Delta = K_I/K_{Ic}$ for Mode I lattice strips of varying height. The calculations are performed with Stokes dissipation $b = 0.05$ in the limit $r_c \to a$ by the Wiener–Hopf technique. The stress intensity factor required for crack motion depends strongly upon system height.

Here a is the lattice spacing, and accounts for the fact that differences between neighboring atoms have been replaced by spatial derivatives. In steady state, time derivatives can be replaced by spatial derivatives, and near a crack tip, $u \sim \sqrt{r}$. Thus the dissipation scales as

$$\dot{\mathcal{E}} \sim \int drrr^{-1/2}a^2\beta r^{-5/2} = a^2\beta \int dr\, r^{-2} \to \infty. \tag{40}$$

This estimate is a bit hasty, since it neglects the angular factors that normally allow energy integrals in fracture dynamics to converge, but the conclusion is correct. Any nonzero level of Kelvin dissipation leads to a divergent energy loss near the tip of a crack. Note however, in the calculations above, that a coefficient β in the microscopic model leads to a coefficient $a^2\beta$ from a macroscopic point of view. Since continuum mechanics is only valid in the limit where $a \to 0$, the coefficient of Kelvin dissipation appears to vanish from a continuum perspective. By choosing the magnitude of β so that the forces due to Kelvin dissipation at the crack tip are of the same order of magnitude as other terms, its contribution in the bulk far from the tip is negligible.

Changing the values of microscopic dissipation parameters has noticeable effects upon fracture. Dissipation at the microscopic level damps down small-scale atomic vibrations and stabilizes crack motion. Cracks are stable over a larger range of loading. In this respect, microscopic dissipation actually makes materials more brittle, a point previously noted by Holian and Ravelo (1995). Figure 13 shows how crack dynamics depend upon the level of Kelvin dissipation for the ideal brittle solid with $r_c = 1.2a$. Increasing β increases the range of Δ over which the crack is stable, and diminishes the size of the velocity gap. The upper critical velocity at which steady states become unstable changes rather little.

It is interesting to ask what would happen if the level of Kelvin dissipation became much larger than 1, and some results are displayed in Figure 14. The whole structure of the v-Δ

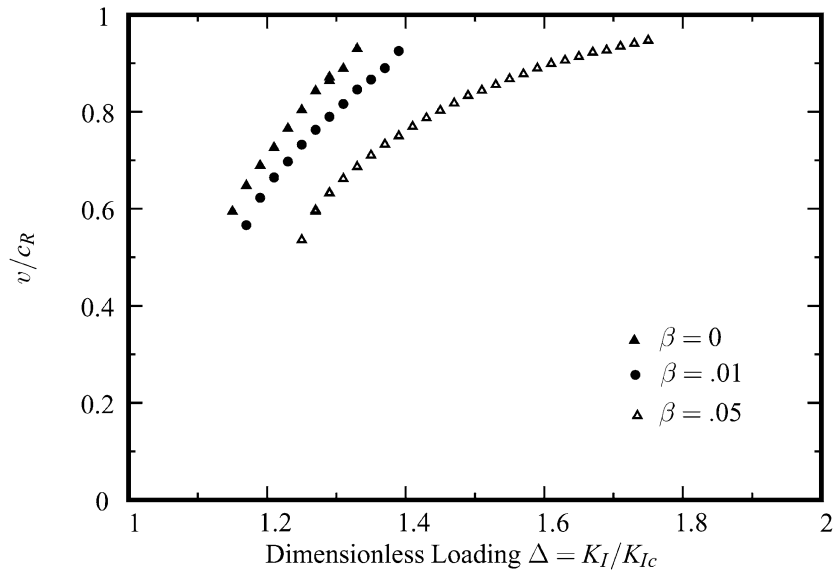

Figure 13. Crack velocity v versus loading Δ for cracks in lattices $N = 60$ rows high with $r_c = 1.2a$ and various values of Kelvin dissipation β.

curve changes. The velocity gap is gone, and fractures can travel arbitrarily low speeds. This observation is consistent with the existence of the velocity gap at lower values of dissipation, because the first fractures begin to run when Δ reaches the value where lattice trapping ends. Over a range of Δ from 2 until 2.25, which could easily be controlled experimentally, such cracks travel at less than 10% of the sound speed. Brittle materials do not behave in this way.

4.5. Rotations

4.5.1. *Violation of the principle of local symmetry*

The theory of fracture mechanics largely concerns itself with the properties of cracks traveling in straight lines. The theoretical attention that has been devoted to crack direction is less than has been devoted to initiation conditions, and speed along a straight line. When a crack turns away from a straight path, some criterion must be employed to choose its direction. The *principle of local symmetry* states that cracks travel in a direction such that $K_{II} = 0$, and is usually employed for this purpose (Goldstein and Salganik, 1974). Many different arguments lead to the conclusion that the principle of local symmetry is sensible, including calculations to maximize energy release, dynamical rules that prevent the crack tip from turning instantaneously (Hodgdon and Sethna 1993), and generalized crack-tip forces (Adda-Bedia, et al., 1999), which can be obtained from a variational principle (Oleaga, 2001).

I will now provide a specific example where the principle of local symmetry is not obeyed. The rule $K_{II} = 0$ does not always correctly predict crack paths. Instead there is an interplay between the direction dictated by elastic stresses outside the tip, and the direction dictated by microstructure. I first tried to test this idea by running cracks through strips where the crystal is tilted at an angle with respect to the long direction of the strip. However, such runs are were not conclusive. The crack always departed from the x axis, and its motion was difficult to characterize with precision. A more compelling demonstration is obtained by finding steady crack motion along the centerline of a strip that is loaded in a mixture of Modes I and II.

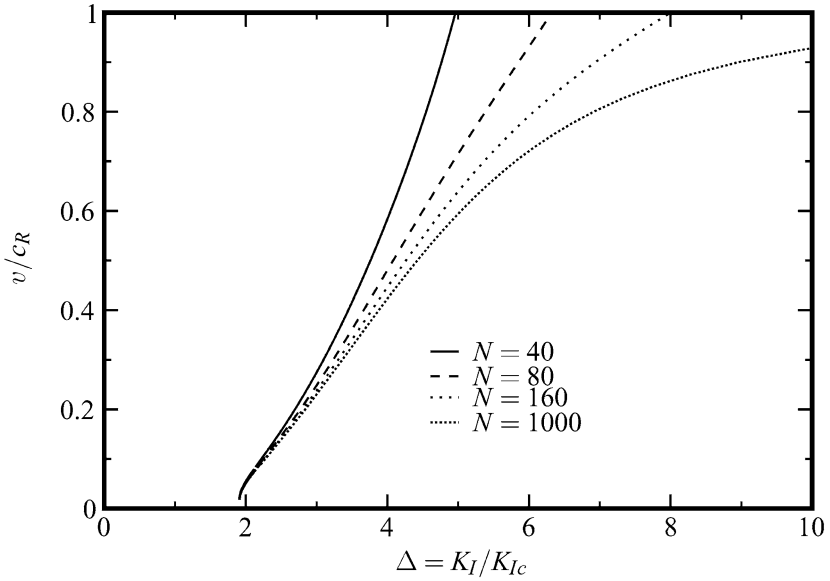

Figure 14. This diagram shows the fracture dynamics that would result if one were to choose Kelvin dissipation $\beta = 100$, in lattices with different numbers N of horizontal rows. The computations are impractical through molecular dynamics, and are performed in the limit $r_c \to a$ by the Wiener–Hopf technique. The macroscopic limit is achieved for lattices much larger than those needed to study the case of small dissipation, and the dynamical behavior of cracks is very different.

The continuum fields surrounding such a crack can be computed exactly, and the condition $K_{II} = 0$ requires them to turn and move off the axis. For example, the cracks in Figure 15 travel in lattices where the upper boundary is rigidly displaced by amounts (δ_x, δ_y), where $\delta_x/\delta_y = \tan(.073\pi)$. The figure shows contours of stress computed directly from atomic positions. These computations are performed by taking binned spatial averages in volumes V_0 of

$$\sigma_{\alpha\beta} = \frac{1}{4V_0} \sum_j [r_{ij}^{\alpha} f_{ij}^{\beta} + r_{ij}^{\beta} f_{ij}^{\alpha}], \tag{41}$$

where $\vec{f}_{ij}$ is the force between atoms i and j (Lutsko, 1988). In the case of Figure 15(B) the system is not large enough for the $1/\sqrt{r}$ stress field to be fully visible, but the atomic configurations very near the crack tip have reached their final form and do not change appreciably as the system becomes larger.

On the other hand, using the known mixed-mode loading conditions and the observed speed of the crack, one can use linear elastic fracture mechanics to compute the universal stress fields that should surround the tip. The shear and hoop stresses predicted to surround the tip of the crack in Figure 15(B) are shown in Figure 4.5.1. According to the principle of local symmetry, the cracks in Figure 15 should rapidly turn in move in the direction such that K_{II} vanishes; these directions are indicated by an arrow in Figure 15. However, the cracks do not move in this direction. They continue forever along the horizontal axis, trapped on a crystal plane. It is worth emphasizing once again that the continuum elastic theory for the systems shown in Figure 15 is completely isotropic. Rotational symmetry is only broken below scales where continuum theory applies, and therefore one must turn to these smaller scales in order to predict crack paths.

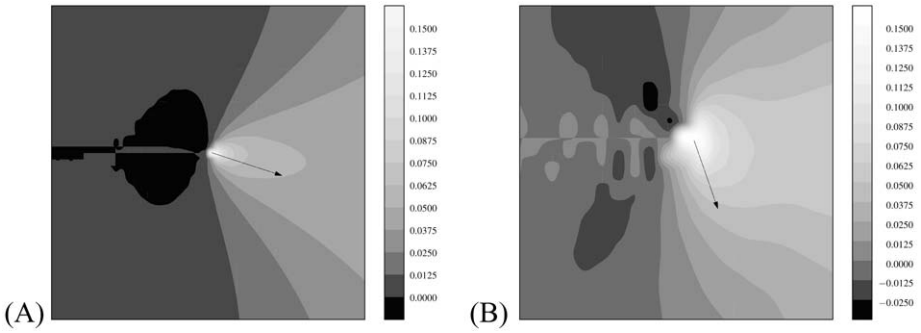

Figure 15. Hoop stress field $\sigma_{\theta\theta}$ surrounding crack tips traveling under mixed-mode loading with $\delta_x/\delta_y = \tan(.073\pi)$. The arrows indicates the directions the cracks would be predicted to turn according to the principle of local symmetry, $K_{II} = 0$. Instead, the cracks travel in steady state along the horizontal axis. (A) Run in triangular lattice 149 rows high, with $r_c = 1.2$ and Kelvin dissipation $\beta = 2$, resulting in a crack velocity $v/c_R = .01$. (B) Run in triangular lattice 199 rows high, with $r_c = 1.2$ and Kelvin dissipation $\beta = .02$, resulting in a crack velocity $v/c_R = .83$.

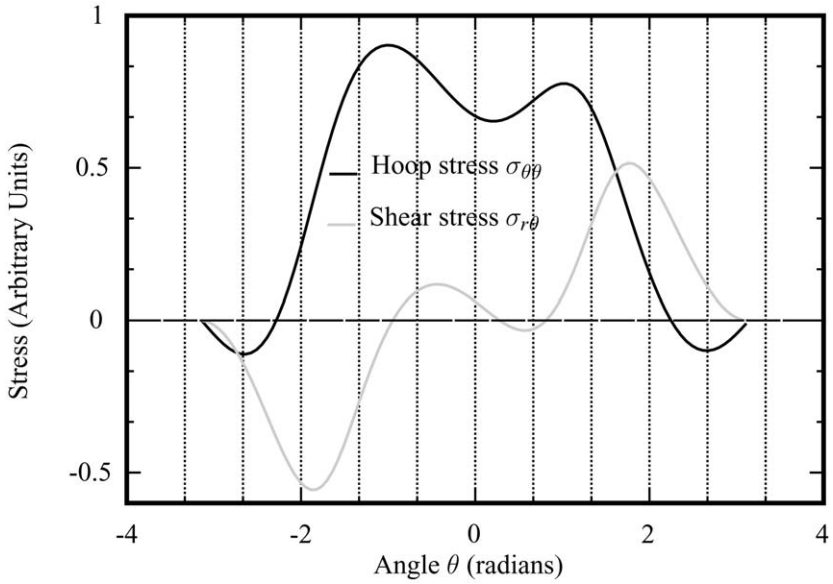

Figure 16. Theoretical hoop stress $\sigma_{\theta\theta}(\theta)$ and shear stress $\sigma_{r\theta}(\theta)$ around crack tip for crack traveling at speed $v/c_R = .83$ under the mixed mode loading applied to the crack in Figure 15(B).

It is natural to wonder for what range of mixed-mode loading horizontally traveling cracks remain stable. Some information on this question is provided in Figure 17. The answer depends upon the coefficient of Kelvin dissipation β. As β increases from zero, the range of mixed-mode loading for which horizontally-traveling cracks are stable increases. This observation by itself indicates that it will be difficult to formulate a criterion within linear elastic fracture mechanics to predict crack paths, since Kelvin dissipation must vanish in any continuum description of sharp cracks. Nevertheless, in the next subsection, I will to attempt to explain these results from the viewpoint of continuum theory.

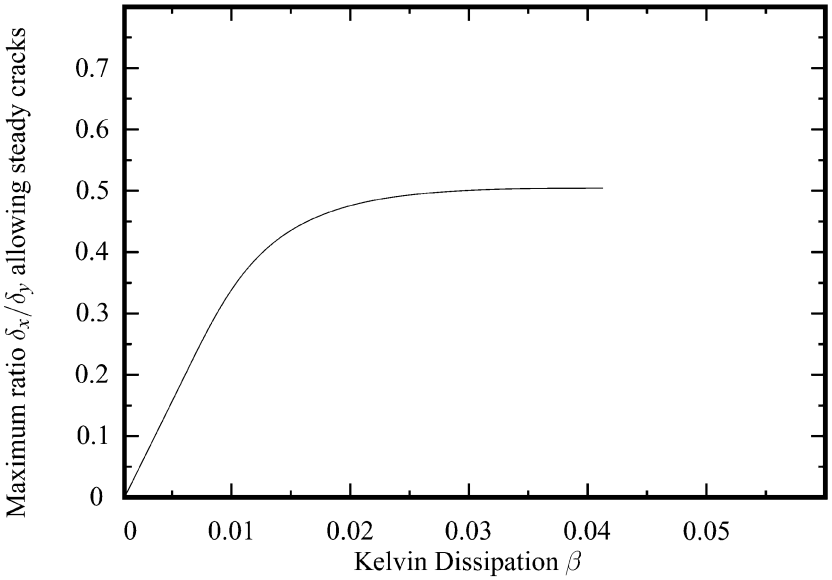

Figure 17. Phase diagram showing combinations of Kelvin dissipation and mixed-mode loading that permit steady motion down center of strip. Cracks with shear loading and dissipation below the line in this figure travel stably along the horizontal axis, while those above it deviate from the horizontal axis. The computations begin with pure Mode I loading at $\Delta = \Delta_I = 1.29$, and then increase the horizontal displacement of the upper boundary δ_x while keeping the vertical displacement δ_y fixed.

4.5.2. *Generalizing the principle of local symmetry*

The principle of local symmetry does not explain the results depicted in Figure 15. Perhaps a simple modification of the usual rule could do so. In a crystal, the energy per area $\Gamma(\theta)$ a crack needs to create new surfaces depends upon the angle θ between the crack and crystalline planes. In an amorphous material, there should be no such angular dependence of surface energy. This observation suggests modifying the principle of local symmetry to choose a crack direction that maximizes the difference between energy flowing to the crack tip along θ and energy required along θ to create new surfaces.

By returning to the derivations of Adda-Bedia et al., (1999) and Oleaga (2001) it is possible to generalize the principle of local symmetry in this fashion. This generalization does capture the tendency of cracks in crystals to move along crystal planes. However, it does not explain quantitatively the results in Figure 15. In particular, I have found no way to account even qualitatively for the results in Figure 17 from a continuum point of view.

One must discuss the methods used to form a correspondence between linear elastic fracture mechanics and the calculations in Figure 15. The first task is to compute the stress intensity factors K_I and K_{II}. This task is most easily accomplished by considering energy balance. The energy G available per length for crack motion is

$$G = \frac{1}{2h}\left[(\lambda + 2\mu)\delta_y^2 + \mu\delta_x^2\right], \tag{42}$$

where h is the height of the strip as in Figure 1. This expression can be compared with the result for energy per length flowing to a crack tip [7]

$$G = \frac{v^2}{2\mu c_s^2 R}\left[\alpha_l K_I^2 + \alpha_s K_{II}^2\right]; \quad \alpha_i = \sqrt{1 - v^2/c_i^2}; \quad R = 4\alpha_l\alpha_s - (1 + \alpha_s^2)^2. \tag{43}$$

Setting Equations (42) and (43) equal gives

$$K_I = \sqrt{\frac{\mu c_s^2 R(\lambda + 2\mu)\delta_y^2}{hv^2\alpha_l}}; \quad K_{II} = \sqrt{\frac{\mu^2 c_s^2 R\delta_x^2}{hv^2\alpha_s}}. \tag{44}$$

To generalize the principle of local symmetry, I return to its derivation for dynamic cracks by Adda-Bedia *et al.* (1999) and Oleaga (2001). They use Eshelby's energy-momentum tensor to compute an energy flow vector $\vec{G}$. The component of this vector parallel to the crack tip, $G_\parallel$ is precisely the energy flux defined in Equation (43):

$$G_\parallel = G = \vec{G} \cdot \hat{e}_\parallel, \tag{45}$$

where $\hat{e}_\parallel$ is a unit vector pointing along the current direction of the crack tip. The component of $\vec{G}$ perpendicular to the crack tip is given by considering energy changes due to small virtual displacements of the crack tip in a direction perpendicular to $\hat{e}_\parallel$ and is

$$G_\perp = \frac{1}{\mu R^2}\alpha_s\alpha_d(\alpha_s - \alpha_d)(\alpha_s^4 - 1)K_I K_{II}. \tag{46}$$

So, to sum up,

$$\vec{G} = \hat{e}_\parallel \frac{v^2}{2\mu c_s^2 R}\left[\alpha_l K_I^2 + \alpha_s K_{II}^2\right] + \hat{e}_\perp \frac{1}{\mu R^2}\alpha_s\alpha_d(\alpha_s - \alpha_d)(\alpha_s^4 - 1)K_I K_{II}. \tag{47}$$

Oleaga and Adda-Bedia *et al.* derive different equations of motion for cracks from this force. Oleaga's equation seems more firmly grounded, and I follow his procedure, but generalize it to the case where the energy per area required for crack motion, $\Gamma(v, \theta)$ depends both upon crack speed (which Oleaga considered) and upon the angle θ between the crack tip and crystalline planes (which he did not).

Crack motion is determined by two conditions. First, the energy flux to the crack tip must equal the energy consumed when a crack extends in that direction. Let θ_c describe the angle from the horizontal axis along which the crack, and $\hat{e}_\parallel$, are currently pointing. Then

$$\Gamma(v, \theta_c) = \hat{e}_\parallel \cdot \vec{G} = G \tag{48}$$

Second, the direction of crack motion is the direction in which energy flux minus energy consumption is maximum. To be precise, let θ describe an arbitrary angle measured from the horizontal axis. Along the actual direction of crack motion, energy flux equals energy consumption, so along any other direction the energy required for the crack to move must be greater than the energy arriving:

$$\Gamma(v, \theta) \geq [\cos\theta\hat{x} + \sin\theta\hat{y}] \cdot \vec{G}. \tag{49}$$

Equations (48) and (49) are sufficient to determine crack speed and direction, and they generalize the principle of local symmetry to include microscopic anisotropy.

If the fracture energy Γ is independent of angle θ, Equations (48) and (49) lead to the conclusion that the crack must travel so that $G_\perp = 0$. This can be demonstrated by supposing the contrary; if the vectors $\vec{G}$ and $\hat{e}_\parallel$ are not parallel, there is always some virtual direction of crack motion that will violate the inequality in (49), as illustrated in Figure 18(A). Normally, $G_\perp = 0$ might be assumed to imply that $K_{II} = 0$, but it is the product $K_I K_{II}$ that must

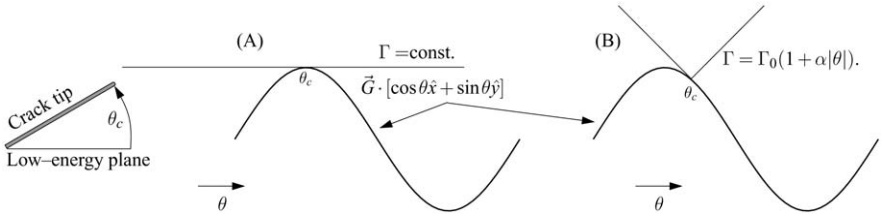

Figure 18. (A) When fracture energy is independent of direction, the only way to satisfy Equations (48) and (49) is for $\vec{G}$ to be parallel to $\hat{e}_{\|}$ so that varying θ always makes the right hand side of Equations (49) decrease. (B) If fracture energy has a cusp-like minimum, then there are many ways to satisfy Equations (48) and (49). At the point where the two curves touch, one needs the slope of the right hand side of Equation (49) to be less than the slope of $\Gamma(\theta)$. A similar graphical construction, suggested by experimental data, is found in Deegan et al. (2003).

vanish. Sutton et al. (2000) provide some experimental data for cracks growing along a line where $K_I = 0$ instead.

When $\Gamma(\theta)$ is not constant matters are even more complicated. In particular, let θ describe the angle between $\delta\hat{e}$ and a weak crystal plane occupying the $\hat{x}$ axis, and suppose that Γ has the dependence expected for small angles θ in the presence of crystal planes

$$\Gamma(\theta) = \Gamma_0(1 + \alpha|\theta|), \tag{50}$$

where $\alpha > 0$ is a constant of order unity and Γ_0 is the fracture energy along the plane. For small θ, Equation (49) now implies

$$(\cos\theta - 1)\Gamma_0 + \sin\theta G_\perp < \Gamma_0\alpha|\theta| \tag{51}$$

Instead of specifying a direction implicitly through $K_{II} = 0$, Equation (51) describes range of off-axis loading for which propagation along the fracture plane should be stable. A graphical construction indicating how to use Equations (48) and (49) to determine crack direction appears in Figure 18. Consulting (B), one sees that the crack direction is determined by sliding a sharp tip over a sine curve so that the two always remain in contact. The solutions divide in general into two regions. In the first region, the slope of the sine curve is less than $\Gamma_0\alpha$ at the point where Equation (48) is obeyed. For this set of solutions, the tip of the surface energy curve Γ touches the sine curve, meaning that the crack moves in direction $\theta = 0$ although $\vec{G}$ does not point in this direction and $K_{II} \neq 0$. There is another set of solutions where $\Gamma(\theta)$ is tangent to the sine curve. For these solutions the crack direction θ is continuously variable, but still one does not have $K_{II} = 0$.

Hodgdon and Sethna (1993) proposed a modification of the principle of local symmetry. They do not allow crack tips to turn instantaneously, but instead write down a differential equation that directs the crack tip to turn continuously, reaching the direction imposed by local symmetry over a length scale f. An equation of this type employing Equations (48) and (49) is

$$\Gamma(v,\theta) \;=\; G_{\|} \tag{52a}$$

$$\frac{\partial}{\partial t}\theta, t, \;=\; -\frac{v}{f}\frac{\partial}{\partial\theta}\left[\Gamma(v,\theta) - (\cos\theta\hat{x} + \sin\theta\hat{y})\cdot\vec{G}\right]. \tag{52b}$$

I believe that Equation (52) is the most plausible candidate for an equation of motion for cracks in crystals based upon continuum reasoning. Its qualitative predictions are consistent

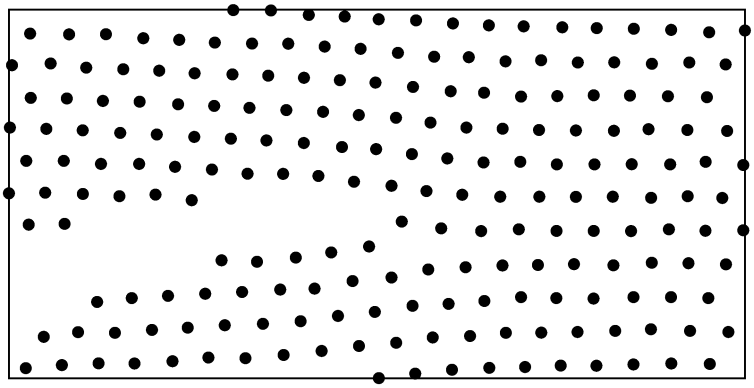

Figure 19. Typical configuration of atoms near crack tip during the course of thermal creep. Notice that a small void has opened up to the right of the main tip, and slightly below it. This configuration traps the crack tip with a higher energy barrier than provided by pure lattice trapping.

with experiment, but it does not predict properties of atomistic simulations quantitatively. For the triangular lattice in this paper, the constant α in Equation (51) is $1/\sqrt{3}$. Thus, neglecting terms of order θ^2 in Equation (51), motion along the horizontal axis should be stable so long as $G_\perp/G_\parallel < 1/\sqrt{3}$. The crack shown in Figure 15(B) has $\delta_x/\delta_y = \tan(.073\pi)$, $v/c_R = .83$ and computing G I find $G_\perp/G_\parallel = 0.068$. According to Equation (52), it should be able to withstand a several-fold increase in $G_\perp$, and in fact for all values of K_{II}/K_I, one finds $G_\perp/G_\parallel < 1/\sqrt{3}$, so the equation of motion predicts that crack motion along the plane is stable so long as the small-angle approximation to the surface energy is valid. However, increasing δ_x by even 10% destabilizes the motion. Since Equation (52) is based purely upon variational principles and energy balance I would not have expected it to make quantitative predictions about the stability of cracks, and it appears not to do so.

4.6. Temperature

Nonzero temperature has two main effects on very brittle cracks. First, it permits them to creep forward at values of Δ that would leave them lattice trapped at zero temperature. Second, it disrupts the steady forward motion of rapidly running cracks, and blunt their tips. That is, the two branches of crack motion, such as shown in Figure 4 respond differently to temperature.

The horizontal branch at $v = 0$ changes to a branch where cracks creep forward at a rate v_c that behaves as (Marder, 1996).

$$v_c \propto \exp\left[-A(\Delta - \Delta_c)^2/k_B T\right], \tag{53}$$

where Δ_c is the value of Δ at which lattice trapping ends, and A is a constant that describes the amount of energy needed to overcome the lattice-trapping barrier. This calculation rested upon the assumption that lattice trapping of a perfectly sharp crack in an otherwise perfect lattice constituted the energy barrier over which a crack had to travel to propagate. In fact, by observing cracks propagating numerically in the presence of a thermal bath, one finds that they frequently generate trapping regions a few atoms in extent, as shown in Figure 19. Therefore, one might expect an expression of the form shown in Equation (53) to be correct, but that A and Δ_c would have to be replaced by a values that reflect the energies of the most important trapping configurations.

To examine this idea, I have performed some computations on the ideal brittle solid. To enforce nonzero temperature, each atom receives random kicks at each time step. The magnitude of the random kicks on an atom depends upon the dissipation affecting the atom according to the fluctuation-dissipation theorem; see Landau and Lifshitz p. 362. If an atom has a Stokes dissipative term of the form

$$-b\dot{\vec{u}}, \tag{54}$$

then it receives kicks of magnitude

$$\vec{\Xi}\sqrt{6bT/dt}, \tag{55}$$

where Ξ is a vector composed of random numbers evenly distributed in the interval $[-1, 1]$. If the force between atoms i and j contains a dissipative Kelvin contribution

$$-\beta(\dot{\vec{u}}_i - \dot{\vec{u}}_j), \tag{56}$$

then the force $\vec{F}_{ij}$ between them acquires a random contribution

$$\vec{\Xi}\sqrt{6\beta T/dt}. \tag{57}$$

Figure 20 represents data obtained by running cracks in thermal baths in two different ways. The raw data showing crack speed versus loading Δ are displayed at various temperatures in (a). In (b), the velocities are rescaled to compare with

$$v = v_0 \exp\left[-B(\Delta - \Delta_t)^2\epsilon/(k_B T)\right], \tag{58}$$

where

$$\epsilon \equiv \frac{1}{2}\kappa(r_c - a)^2, \tag{59}$$

$v_0 = 1.78c_R$, $B = .33$ and the effective trapping Δ_t is given by $\Delta_t = 2.21$. The total energy ϵ needed to break the bond between any two atoms is 0.02, and this value sets the scale on which temperature becomes important. For this reason, ϵ appears in Equation (58), allowing the free parameter B to be dimensionless. It is natural to ask the question whether there is some temperature above which the velocity gap disappears and below which it disappears. This question must be refined if it is to be given a definite answer. The appropriate question is this: at any given temperature, if one starts with a steady state crack, what is the probability that the crack will run a certain length before temperature fluctuations cause it to arrest? I have addressed this question, by executing runs in systems 59 rows high. It is important to begin with a steady-state crack, because the probability for a crack to be arrested by thermal fluctuations changes as one moves from an ignition phase, where large-amplitude waves designed to break the tip free from lattice-trapping are present, to the final steady state. The results of repeated runs with identical initial states but different random seeds for the temperature fluctuations, and different temperatures appear in Figure 21. The time to arrest fits the form

$$t_{\text{arrest}} = t_0 \exp(C\epsilon/k_B T) \tag{60}$$

with $t_0 = 19.4\sqrt{am/\kappa}$ and $C = 0.017$. The time to arrest should depend upon Δ, but I have neither a theoretical nor experimental estimate for it. A theoretical estimate could in principle be obtained from the formalism in Marder (1996).

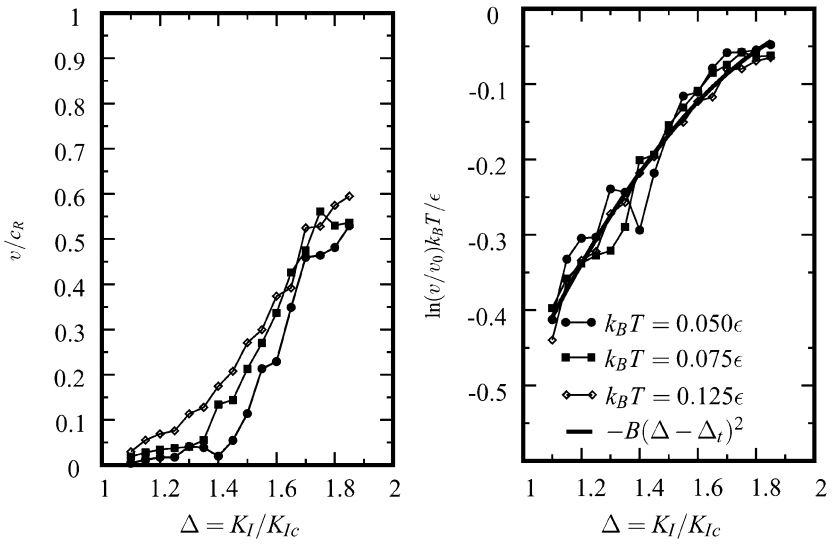

Figure 20. (a) Crack velocity v versus loading Δ as a function of temperature. (b) Same data rescaled as suggested by Equation (58).

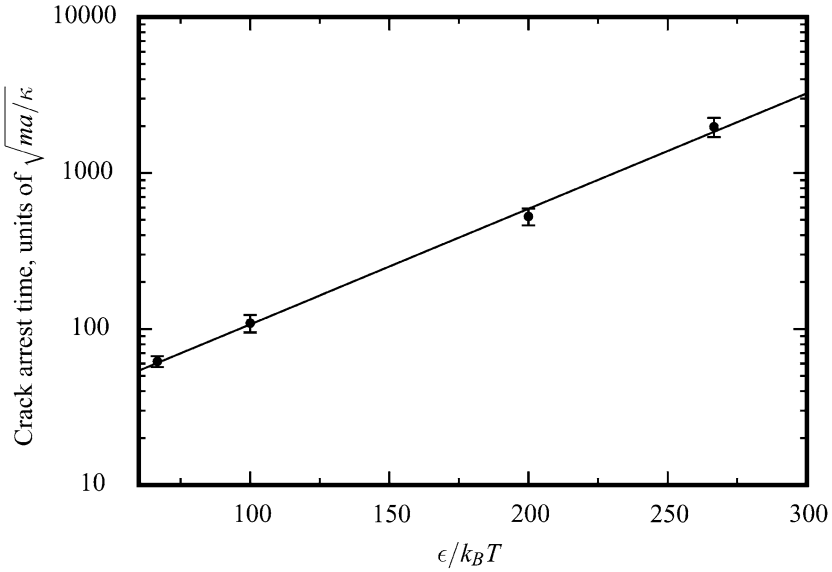

Figure 21. Mean time to arrest for cracks in system 59 rows high, $r_c = 1.2$, Kelvin dissipation $\beta = .01$, and $\Delta = 1.3$. Error bars show standard error. The results are consistent with the form in Equation (60), shown as the solid line.

Any conclusions reached here about the effects of temperature are very dependent upon the fact that the calculations are carried out in two dimensions. The three-dimensional situation is different. The process of creep becomes more complex; portions of the crack line move ahead unevenly because of thermal fluctuations, and eventually the rest of the crack line follows (Hsieh and Thomson, 1973, Sinclair, 1975, Markworth and Hirth, 1981, Lin and Hirth, 1982, Thomson et al. 1987, Marder, 1998). Just as thermal fluctuations have a harder time moving a stationary crack front forward in three dimensions than two, they probably have a more difficult time disrupting a rapidly moving front. Some three-dimensional calculations

at nonzero temperature are contained in Holland and Marder (1999), but the issue of crack motion in three dimensions at nonzero temperature has not really been studied in detail.

5. Lennard–Jones solid

The examinations of fracture in this paper have up to this point focused upon particles interacting through short-range ideally brittle force laws. It is interesting to ask what qualitative changes in fracture result when one moves to a softer, longer-range potential. To provide an example, I have investigated briefly a Lennard–Jones solid, first studied in this context by Abraham et al. (1994). This solid is defined by the pairwise interaction energy

$$\phi(r) = \frac{1}{2}\epsilon_0 \left[\frac{1}{12} \frac{g a^{12}}{r^{12}} - \frac{1}{6} \frac{a^6}{r^6} \right] \theta(r_c - r) + \text{const}\, \theta(r - r_c). \tag{61}$$

Here g is chosen to set the equilibrium lattice spacing to a and has numerical value $g = 1.05$, $r_c = 2.5a$, which includes interactions up to second-nearest neighbors, and ϵ_0 is a constant with dimensions of energy. Computing the two-dimensional bulk modulus by carrying out lattice sums gives $\lambda + \mu = 5.47\epsilon_0/a^3$, and subjecting the crystal to uniform strains where only e_{yy} is nonzero gives $\lambda + 2\mu = 7.2\epsilon_0/a^3$. Thus the wave speeds are $c_l = 2.49\sqrt{\epsilon_0/m}$, $c_t = 1.22\sqrt{\epsilon_0/m}$, and $c_R = 1.14\sqrt{\epsilon_0/m}$.

Some results from numerical searches for steady-state cracks appear in Figure 22. There are several qualitative ways that these cracks differ from those in the ideal brittle solid. The region of lattice trapping is extremely small. There is no measurable velocity gap. Characteristic velocities are small compared to those seen previously. The relation between v and Δ contains many plateaus that appear to be completely flat within numerical accuracy. Similar plateaus have been observed in numerical studies of silicon (Holland and Marder, 1999). The range of Δ that allows steady states is very small; for Δ larger than 1.025 there appears to a period-doubling bifurcation of crack speed leading to low-dimensional chaos, and by $\Delta = 1.04$ the crack blunts and stops.

The qualitative lesson to take from these observations is that soft potentials and long-range interactions can greatly reduce the energy transmitted to phonons, and make it possible for dynamic fractures to propagate slowly just above the thermodynamic Griffith point. This qualitative observation deserves to be put on more quantitative basis, and it would be interesting to explain the plateaus in the relation between v and Δ.

6. Conclusions

In bringing this paper to a close, I must acknowledge that the studies performed here raise as many questions than they answer. The goal of the paper was to take a particular system and study its fracture properties carefully. The two-dimensional ideal brittle crystal seemed the appropriate place to start. However, as I probed the robustness of its fracture solutions, it came to seem less like the samples I know from laboratory experiments. The ideal two-dimensional brittle crystal has properties very similar to brittle laboratory crystals only so long as it is treated with great care. Pulling on it too hard can cause running cracks to arrest. Thermal fluctuations can cause running cracks to arrest. Very slight mis-alignment of crystalline axes with the axis of loading can cause running cracks to arrest. If cracks in the laboratory were this delicate, fracture experiments just above the Griffith point would not be possible.

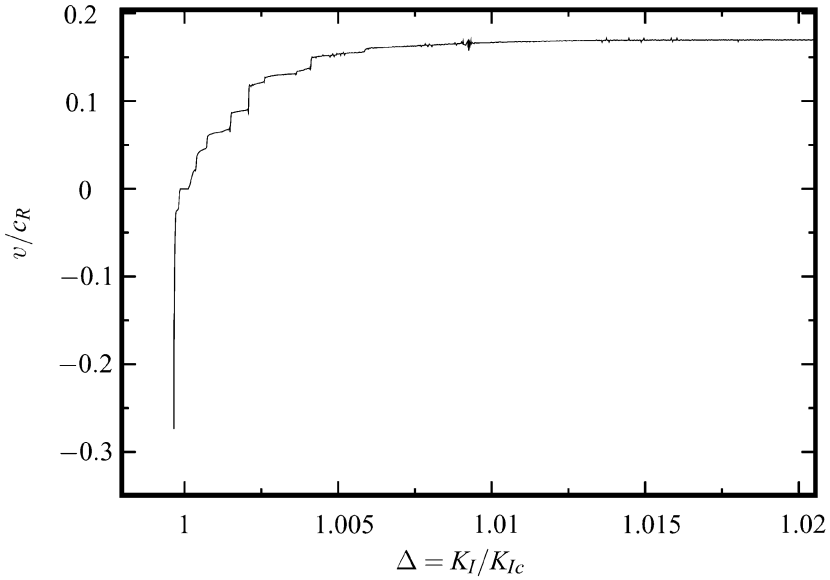

Figure 22. Velocity versus dimensionless loading $\Delta = K_I/K_{Ic}$ for atoms in triangular Lennard–Jones solid interacting out to next-nearest neighbors. The region of lattice trapping is extremely small, and there is no visible velocity gap.

Despite this worry, studies in the ideal brittle crystal suffice to set certain questions to rest. They show conclusively that macroscopic elastic properties and linear elastic fracture mechanics do not contain enough information to predict the direction of crack motion. Supplementing this information about a solid with thermodynamic properties of surface energies is not enough either. To account for the results in Figure 17, one requires information about microscopic dynamics. Thus, I conclude that crack motion depends in great detail upon properties of the process zone, and that macroscopically identical materials can have very different fracture properties. The one caveat that must be expressed is that the models in which these conclusions were reached differ in some ways I have described above from familiar laboratory samples. It could be that when one finds a model that behaves in all respects like laboratory materials, its properties will be less variable that those of the systems I have so far managed to solve.

Acknowledgements

The National Science Foundation (DMR-9877044 and DMR-0101030) supported this work. Patrick Klein suggested the calculation involving the Lennard–Jones solid.

References

Abraham, F. F., N. Bernstein, J. Q. Broughton and D. Hess (2000). Dynamic fracture of silicon: concurrent simulation of quantum electrons, classical atoms, and the continuum solid. *Materials Research Society Bulletin* **25**(5), 27–32.

Abraham, F. F., D. Brodbeck, R. A. Rafey and W. E. Rudge (1994). Instability Dynamics of Fracture: A Computer Simulation Investigation. *Physical Review Letters* **73**(2), 272–275.

Adda-Bedia, M., M. Arias, M. B. Amar and F. Lund (1999). Generalized Griffith criterion for dynamical fracture and the stability of crack motion at high velocities. *Physical Review E* **60**, 2366–2376.

Baskes, M. I. (1992). Modified embedded-atom potentials for cubic materials and impurities. *PRB* **46**, 2727–2742.
Baskes, M. I., J. E. Angelo and C. Bisson (1994). Atomistic Calculations of Composite Interfaces. *Modelling and Simululation in Materials Science and Engineering* **2**, 505–518.
Deegan, R. D., S. Chheda, L. Patel, M. Marder, H. L. Swinney, J. Kim and A. de Lozanne (2003). Wavy and rough cracks in silicon. *Physical Review E* **67**,066209.
Freund, L. B. (1990). *Dynamic Fracture Mechanics.* Cambridge: Cambridge University Press.
Gerde, E. (2001). Fracture and Friction. Ph.D. thesis, The University of Texas at Austin.
Goldstein, R. V. and R. Salganik (1974). Brittle fracture of solids with arbitrary cracks. *International Journal of Fracture* **10**, 507–523.
Griffith, A. (1920). The phenomena of rupture and flow in solids. *Mechanical Engineering* **A221**, 163–198.
Hauch, J., D. Holland, M. Marder and H. L. Swinney (1999). Dynamic Fracture in single-crystal silicon. *Physical Review Letters* **82**, 3823–3826.
Hauch, J. and M. Marder (1998). Energy Balance in Dynamic Fracture, Investigated by a Potential Drop Technique. *International Journal of Fracture* **90**, 133–151.
Heizler, S.I., D.A. Kessler and H. Levine (2002). Mode-I fracture in a nonlinear lattice with viscoelastic forces. *Physical Review E* 66 016126/1-10.
Hodgdon, J. A. and J. P. Sethna (1993). Derivation of a general three-dimensional crackpropagation law: a generalization of the principle of local symmetry. *Physical Review B* **47**, 4831–4840.
Holian, B. L. and R. Ravelo (1995). Fracture simulations using large-scale molecular dynamics. *Physical Review B* **51**, 11275–11288.
Holland, D. and M. Marder (1998a). Erratum (Ideal brittle fracture of silicon studied with molecular dynamics. *Physical Review Letters* **81**, 4029.
Holland, D. and M. Marder (1998b). Ideal brittle fracture of silicon studied with molecular dynamics. *Physical Review Letters* **80**, 746–749.
Holland, D. and M. Marder (1999). Cracks and atoms. *Advanced Materials* **11**, 793–806.
Hsieh, C. and R. Thomson (1973). Lattice theory of fracture and crack creep. *Journal of Applied Physics* **44**, 2051–2063.
Landau, L. D. and E. M. Lifshitz (1980) *Statistical Physics, Part 1*. Oxford: Pergamon Press, third edition.
Lin, I. H. and J. P. Hirth (1982). On brittle crack advance by double kink nucleation. *Journal of Materials Science* **17**, 447–460.
Lutsko, J. F. (1988). Stress and elastic constants in anisotropic solids: Molecular dynamics techniques. *Journal of Applied Physics* **64**, 1152–1154.
Marder, M. (1996). Statistical Mechanics of Cracks. *Physical Review E* **54**, 3442–3454.
Marder, M. (1998). Energies of a kinked crack line. *Journal of Statistical Physics* **93**, 511–525.
Marder, M. and S. Gross (1995). Origin of crack tip instabilities. *Journal of the Mechanics and Physics of Solids* **43**, 1–48.
Marder, M. and X. Liu (1993). Instability in Lattice Fracture. *Physical Review Letters* **71**, 2417–2420.
Markworth, A. J. and J. P. Hirth (1981). An atomistic model of crack extension by kink propagation. *Journal of Materials Science* **16**, 3405–3417.
Oleaga, G. E. (2001). Remarks on a basic law for dynamic crack propagation. *Journal of the Mechanics and Physics of Solids* **49**, 2273–2306.
Sinclair, J. E. (1975). The influence of the interatomic force law and of kinks on the propagation of brittle cracks. *Philosophical Magazine* **31**, 647–671.
Slepyan, L. (1981). Dynamics of a crack in a lattice. *Soviet Physics Doklady* **26**, 538–540.
Slepyan, L. I. (2002). *Models and Phenomena in Fracture Mechanics.* Berlin: Springer.
Spence, J. C. H., Y. M. Huang and O. Sankey (1993). Lattice trapping and surface reconstruction for silicon cleavage on (111). *ab initio* quantum molecular dynamics calculations. *Acta Metallurgica* **41**, 2815–2824.
Sutton, M. A., X. Deng, F. Ma, J. Newman and M. James (2000). Development and application of a crack tip opening displacement-based mixed mode fracture criterion. *International Journal of Solids and Structures* **37**, 3591–3618.
Swadener, J., M. Baskes and M. Nastasi (2002). Molecular dynamics simulation of brittle fracture in silicon. *Physical Review Letters* **89**(8), 085503/1–4.
Thomson, R. (1986). The Physics of fracture. *Solid State Physics* **39**, 1–129.
Thomson, R., C. Hsieh and V. Rana (1971). Lattice Trapping of Fracture Cracks. *Journal of Applied Physics* **42**(8), 3154–3160.

Thomson, R., V. K. Tewary and K. Masuda-Jindo (1987). Theory of chemically induced kink formation on cracks in silica. I. 3-D crack Green's functions. *Journal of Materials Research* **2**, 619–630.

Verlet, L. (1967). Computer 'Experiments' on Classical Fluids. I. Thermodynamical Properties of Lennard-Jones Molecules. *Physical Review* **159**, 98.

Washabaugh, P. D. and W.G. Knauss (1994). A reconciliation of dynamic crack velocity and Rayleigh wave speed in isotropic brittle solids. *International Journal of Fracture* **65**, 97–114.

Willis, J. R. (1967). Crack propagation in viscoelastic media. *Journal of Mechanics and Physics of Solids* **15**, 229–240.

Yoffe, E. H. (1951). The Moving Griffith Crack. *Philosophical Magazine* **42**, 739–750.